University of Thessaly

Department of Mechanical Engineering

Phase Diagrams of Elastic Layer Coated Microbubbles under Insonating Conditions – Effect of Shell Viscosity

By

Vasilopoulos Dionysios

Supervisor Prof. N. Pelekasis

Submitted in partial fulfillment of the requirements for the Diploma of Mechanical Engineering

July 2019

Thesis Committee

1st Member: (Supervisor)	Prof. N. Pelekasis Department of Mechanical Engineering, University of Thessaly
2nd Member:	Assistant Prof. G. Charalampous Department of Mechanical Engineering, University of Thessaly
3rd Member:	Dr. M. Vlachomitrou Department of Mechanical Engineering, University of Thessaly

ABSTRACT

Contrast agents are encapsulated microbubbles that are used in a wide variety of biomedical applications in modern diagnostics and therapeutics. When they are insonated (hit by an ultrasonic acoustic wave) they start oscillating and reflecting a characteristic echo, enhancing the contrast between the blood and the surrounding tissue, thus providing a better visual representation of the medical circumstances at hand.

In the present thesis, phase diagrams of such microbubbles are created, allowing us to observe their behavior when they have different viscoelastic properties as well as when the acoustic stimuli differ. Of the properties discussed later the shear viscosity in particular is of utmost interest. Through consistent studying of the phase diagrams that were constructed during this assignment, valuable information was obtained about how plenty of the microbubbles' properties affect the reaction they have towards an insonifying stimulus. By acquiring better understanding of the way that the contrast agents operate, we might be able to further the technological advances and creating more suitable contrast agents or expanding the range of applications in the biomedical field.

TABLE OF CONTENTS

TABLE OF VARIABLES

R	Radius of the Microbubble
$\dot{R}$	Velocity of the Membrane
$\ddot{R}$	Acceleration of the Membrane
ω	Forcing Frequency
G_s	Surface Shear Modulus
K_b	Bending Elasticity
B	Dimensionless Bending Elasticity
δ_{sh}	Membrane Thickness
ρ_l	Liquid Density
μ_l	Liquid Dynamic Viscosity
P_{st}	Static Pressure
P_∞	Pressure of the Far Field
ε	Amplitude of the Pressure Wave
ΔF_n	Normal Component of the Residual Elastic Stress
σ	Mean Surface Tension between the Gas and the External Liquid
Φ	Velocity Potential
V_G	Dimensionless Instantaneous Volume
γ	Polytropic constant
ξ	Lagrangian variable identifying different points along the surface
We	Webber Number
Re_l	Reynolds Number of the surrounding Liquid
Re_s	Reynolds Number for Dilatational Viscosity
Re_{shear}	Reynolds Number for Shear Viscosity
ν	Poisson Ratio
τ	In-plane Viscoelastic Tension Tensor
s,φ	Radial and Azimuthal Directions respectively
q	Transverse Shear Tensor
k_{bdim}	Scalar Bending Modulus
P_G	Pressure inside the Microbubble
r_d	Position Vector of a Material Point on the Surface of the Bubble
r_0,θ_0	Spherical Coordinates of the Particles Initially
κ_m	Mean Curvature of the Microbubble's Interface
κ_1,κ_2	Curvatures in the principal directions
μ_{sk}	Dilatational Viscosity of the Membrane
μ_{shear}	Shear Viscosity of the Membrane
w,u	Radial and Azimuthal displacement of the membrane respectively
n	Eigenmode Number
λ_1,λ_2	Elongation of line elements in the principal directions
S,s	Lengths of line elements in the referenced and the deformed state

LIST OF FIGURES

	compression on the rest radius.
Figure 8 a,b,c,d	Phase Diagrams for the dynamic response subject to an external acoustic disturbance of a contrast agent insonated at 1.2MHz, with viscoelastic shell properties $Gs=160*10^6$ N/m^2, μ_s=20 Pa*s and (a) μ_{shear}=1 Pa*s without applying any prestress, (b) μ_{shear}=1 Pa*s with the application of a 8.3% initial compression on the rest radius, (c) μ_{shear}=20 Pa*s without applying any prestress and (d)) μ_{shear}=20 Pa*s with the application of a 8.3% initial compression on the rest radius.
Figure 9 a,b,c,d	Phase Diagrams for the dynamic response subject to an external acoustic disturbance of a contrast agent insonated at 1.7MHz, with viscoelastic shell properties $Gs=160*10^6$ N/m^2, μ_s=20 Pa*s and (a) μ_{shear}=1 Pa*s without applying any prestress, (b) μ_{shear}=1 Pa*s with the application of a 8.3% initial compression on the rest radius, (c) μ_{shear}=20 Pa*s without applying any prestress and (d)) μ_{shear}=20 Pa*s with the application of a 8.3% initial compression on the rest radius.
Figure 10 a,b,c,d	Phase Diagrams for the dynamic response subject to an external acoustic disturbance of a contrast agent insonated at 1.2MHz, with dilatational viscosity μ_s=20 Pa*s at radius=3.6μm and (a) $G_s=40*10^6$ N/m^2 without applying any prestress, (b) $G_s=40*10^6$ N/m^2 with the application of a 16.9% initial compression on the rest radius, (c) $G_s=80*10^6$ N/m^2 without applying any prestress and (d)) $G_s=80*10^6$ N/m^2 with the application of a 12.8% initial compression on the rest radius.

ACKNOWLEDGEMENTS

First of all, I would like to express my gratitude towards my thesis supervisor Professor Nikos Pelekasis for taking me under his wing and therefore allowing me to further my knowledge and education on a subject that is extremely interesting as well as useful. I would also like to thank him for always being present when needed and for giving me guidance every single time I was facing difficulties. His patience and good will towards me are greatly appreciated and is what allowed me to complete the present piece of work as effortlessly as possible.

Next, I would really like to thank Dr. Maria Vlachomitrou for helping me and supporting me during my time working and completing my thesis. Without her guidance and advice I would not be able to proceed as smoothly as I did and she provided great help in understanding and figuring out the ForTran code required. The door to her office was always open for me and I can't help but feel indebted for all her help.

I would also like to thank Assistant Professor Georgios Charalampous for taking the time to serve as part of my thesis committee and for reading my thesis.

Lastly, I would like to thank my family and my friends for being there for me every step of the way and provided countless, unforgettable moments of laughter and joy. Always in good spirits, they kept me going when things were tough and I am truly thankful for every single one of them.

I would like most of all to thank my parents for always supporting me and providing me with this wonderful opportunity to learn and better myself. I could not have asked for more. I am forever grateful to them.

1. INTRODUCTION

1.1. General Background

Ultrasound contrast agents are encapsulated microbubbles, 1 to 5 μm in radius and were originally developed for diagnostic imaging purposes. The agents have a gas core and are surrounded by a shell made from a variety of materials. Currently, polymer, lipid and protein materials are used for shell construction in prototype and approved agents. When driven acoustically, the agents have unique scattering signatures from the nonlinear oscillations about their equilibrium radii. [3]

One of the main functions of contrast agents is that they are used in ultrasound imaging to enhance the contrast between the blood pool and the surrounding tissue as a result of the high echogenicity of the microbubbles. Tissue reflects the sound waves at the fundamental frequency so by taking advantage of the nonlinear backscattering properties of the contrast agents the contrast between the blood and the tissue is heightened. [4]

Because of their high echogenicity and their ability to reflect a characteristic echo when caught in an ultrasonic frequency field, these targeted agents can be detected by an ultrasound system with high sensitivity. Therefore they can provide important information when used in biomedical scanning applications such as the spatial distribution and extent of tumor angiogenesis, its inflammatory response or thrombus. [5]

Additionally, microbubbles have the ability of focusing and concentrating energy, forces and stresses and that leads to a variety of phenomena caused by them like cavitation damage, sonoporation and sonoluminescence [11]. Sonoporation is the process by which micropores are generated on the surface of membranes by the application of sound waves. In this fashion microbubbles can be used for therapeutic applications instead of cell wall permeation techniques such as electroporation. [6]

During the application of ultrasonic excitation, microbubbles have been observed to merge, fragment, crack and jet. The jetting phenomenon can be described as follows. When the insonification occurs, during the maximum expanse phase of the microbubble, it collapses due to the vast difference between the pressure inside the bubble and the atmospheric pressure. [13] If there is a boundary near the bubble when it breaks, the water flow on the side of the boundary gets retarded and due to pressure difference between the side of the bubble close to the boundary and its opposite side the fluid volume gets accelerated and focused to the formation of the jet causing the jetting phenomenon. [7],[9]

The pressure at the tip of the jet is high enough to penetrate any human cell so it is presumed that the liquid jet might be able to act as a microsyringe delivering a drug to a region of interest. [7]

The contrast agents disappear after a while once they’ve been inserted in the human body through various mechanisms such as getting captured by lungs and other organs, gas diffusion or dissolution. The destruction mechanisms of the contrast agents depend heavily on their type. [8]

1.2. Types of Shells Used to Coat Microbubbles

Protein Shells

One of the most well known proteins that is used to coat microbubbles, meant to be used in contrast sound imaging, is Albumin. When it was first introduced as a formulation it was considered revolutionary and it functioned as the prototype after which plenty of other formulations were created that could pass the lung capillaries and provide contrast in the left ventricle of the heart. [12] The procedures through which Albumin-coated microbubbles are created involve sonication and thermal processing. Sonication helps to create the air bubble and the heating helps to keep it together. [10]

Apart from Albumin, several other proteins are used to create coated microbubbles. The amphipathic nature of most proteins makes them highly surface active which is a very desirable trait for contrast agents to have.

Surfactant Shells

Surfactants are compounds that lower the surface tension (or interfacial tension) between two liquids, between a gas and a liquid, or between a liquid and a solid. One pretty well known mixture of surfactants that is used to coat microbubbles is that formulated by Wheatley et al. and is a combination of SPAN-40 and TWEEN-40. The solution was sonicated in the presence of air to form stable microbubbles.

It was recently reported by Dressaire et al. that stable microbubbles managed to be formed from sucrose stearate by a blending process in a certain type of glucose syrup. These microbubbles were suspended for over a year and they demonstrated exceptional polygonal domains. [15] It is suggested that this unique domain morphology is due to the interplay between surface tension, domain boundary line tension and spontaneous curvature of the surfactant monolayer. Despite them not being suitable for biomedical implementations due to them being unstable upon dilution, the importance of surface heterogeneity and domain bending with regard to microbubble stability becomes clear through their study. [10]

Lipid Shells

Lipid-coated microbubbles are some of the most useful and remarkable formulations used in biomedical applications and drug delivery. The shell is nature inspired since most microbubbles that are found directly in the environment such as the oceans are known to be stabilized by lipids [16]. Also its stability and compliance matches that of lung surfactant. Two examples of the most widely used contrast agents coated by lipid shells are Definity by Lantheus Medical Imaging and Sonovue® by Bracco Diagnostics. [10]

Lipid shells have a plethora of advantages. One of them is that a lipid monolayer can be spontaneously formed around a bubble of air, since their hydrophobic acyl chains face the gas and their hydrophilic headgroups face the water [14]. In addition, lipid monolayers are highly cohesive thus increasing the stability of the shell and the lipid molecules are held together by ‘weak’ physical forces which makes the shell compliant to area expansion and compression during ultrasound insonification. Due to all the aforementioned reasons the lipid coated microbubbles possess favorable ultrasound characteristics for example they exhibit minimal

damping at resonance. They're also easily functionalized for drug delivery and molecular imaging. [10]

Polymer Shells

The term "polymer microbubble" typically refers to a type of microbubbles that are stabilized by a thick shell that consists of different kinds of polymers which makes it more resistant to area compression and expansion, in comparison with the lipid or albumin ones but in turn reduces their echogenicity and drug delivery activity. The polymer shelled microbubbles have been observed to crack under insonification thereby releasing the content of their core through the shell defect. [10]

An additional categorization that applies for the membrane that surrounds the microbubble is whether its material is strain softening or strain hardening. If its elasticity modulus increases during expansion it is considered as strain hardening [1]. If its elasticity modulus decreases during expansion then it is considered as strain softening. The elasticity modulus characterizes the resistance of the shell to deform. Possible examples of strain hardening materials are the membrane of the red blood cells as well as certain polymers used to coat contrast agents. One example of strain softening material is rubber.

In mathematical modeling of the membranes used in simulating the contrast agents in a computational environment, different constitutive laws are applied in order to account for the fact that the material being tested is strain softening or hardening. The Skalak law is used to describe strain hardening membranes and the Mooney-Rivlin law is used for strain softening membranes. [1]

2. METHODOLOGY

The main purpose of this thesis is the construction of the phase diagrams of strain-softening contrast agents that are subjected to a variety of different acoustic stimuli. Doing a parametric analysis of the results and through careful observation a few important conclusions can be drawn that show how each parameter affects the dynamic behavior of the contrast agent in question.

The Phase diagrams of this particular assignment are constructed in the R_0-ε plane, and define the regions that instabilities occur. The instabilities that are examined are the Excitation of Shape Modes through Static Buckling, Dynamic Buckling and Parametric Mode Excitation. The method used to create these diagrams was to estimate the sound amplitude for which shape mode excitation was taking place depending on the viscoelastic and geometrical characteristics of the shell and the bubble as well as the frequency of the acoustic disturbance. Phase diagrams are extremely helpful because they depict the stability patterns of certain contrast agents under the effect of a specific forcing frequency, thus allowing the prediction of its behavior and in turn its manipulation.

A contrast agent subject to an acoustic disturbance of a certain sinusoidal form with given forcing frequency starts pulsating. In the beginning, for low sound amplitude and after a small transient period has elapsed, the contrast agent undergoes spherosymmetric oscillations assuming that the oscillations are stable. In case stability is not taking place, the microbubble's pulsating morphology changes and it pulsates assuming different deformed shapes. Depending on the size of the bubble as well as the sound amplitude of the forcing frequency the shape of the microbubble is different. The different shapes that the microbubble turns into are categorized as shape modes. In the image below the first shape modes can be depicted so that the reader can have a more accurate understanding of what the different shapes and geometry of the eigenmode look like.

Such mode excitation that is associated with an acoustic disturbance is referred to as parametric shape mode excitation. Besides this mechanism shelled microbubbles may be destabilized statically by simple imposition of a certain uniform and constant pressure disturbance. This process is known as static buckling and typically occurs at higher amplitudes of the pressure disturbance in comparison with parametric instability [1]. In the present study it will be seen how these attributes are affected when the shell is already under stress at the time of the disturbance or when the shell rheology is altered. In particular the impact of a measurable discrepancy between shear and dilatational shell viscosity on microbubble stability will be investigated.

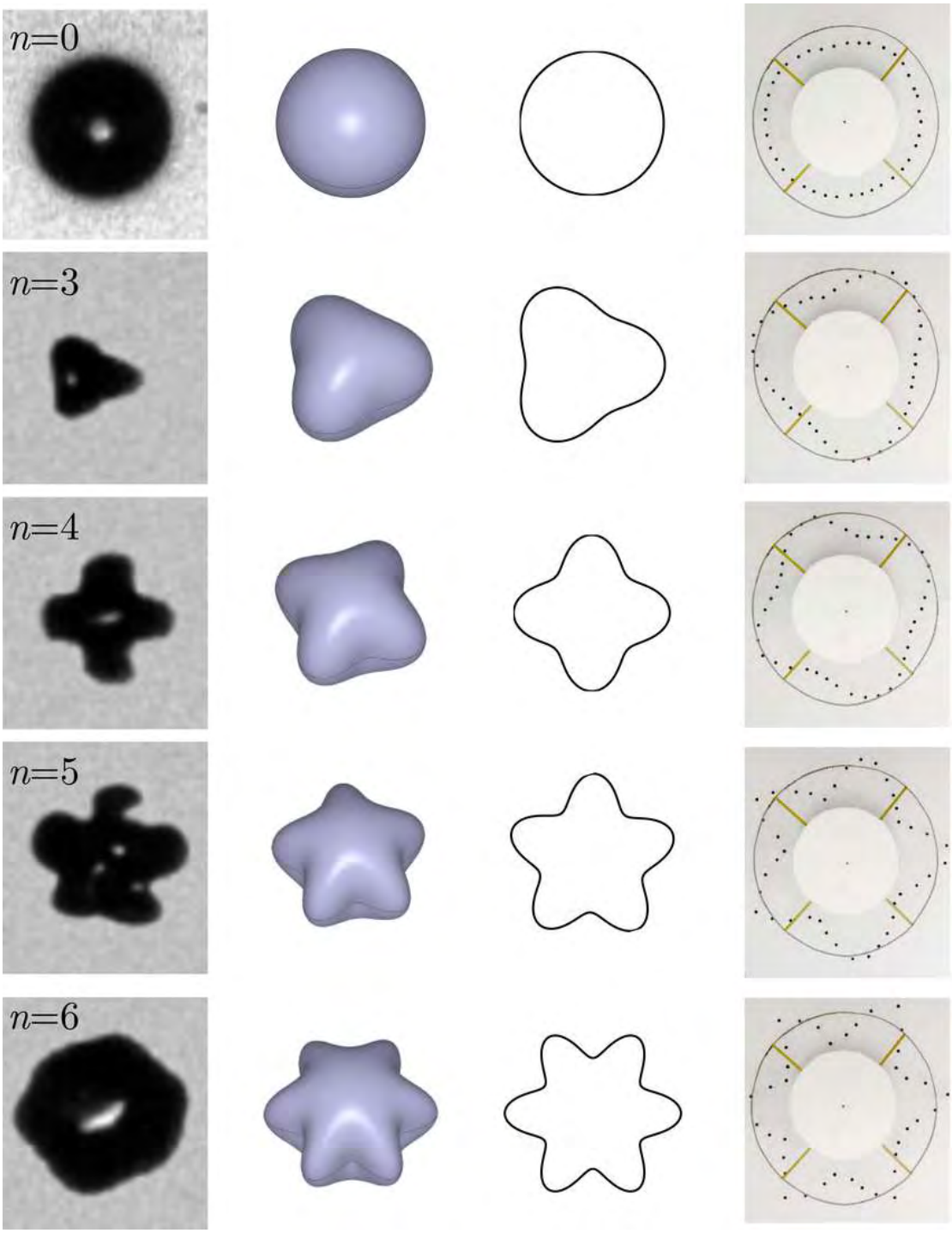

Picture 1: The shapes of a pulsating microbubble while no mode is present as well as when the 3rd, 4th, 5th and 6th modes are excited.

2.1 Formulation

It is of particular interest to examine the phase diagrams of the contrast agents' eigenmodes and observe how those are affected when the shear and dilatational viscosities are of the same value or differ [17], as well as by the existence of pre-stress. In order for that to happen the model presented by Dr. Tsiglifis and Dr. Pelekasis has been enriched with the addition of terms and equations that consider both of the existing viscosities. The mathematical model as well as the numerical methods that are used to carry out this assignment are based on the work done previously by Tsiglifis & Pelekasis [1],[2].

An encapsulated microbubble can be described as a spherical configuration of ideal gas that is enclosed in a viscoelastic membrane of small thickness δ_{sh}, in comparison with its radius. Some of their properties include: the equilibrium radius R_{eq}, the membrane's surface shear modulus, its bending elasticity k_B as well as its shear and dilatational viscosities μ_{shear} and μ_{sk} respectively. The microbubble is also submerged in a Newtonian liquid of density ρ_l dynamic viscosity μ_l and static pressure P_{st}. [1][2]

The Reynolds number used to describe the interaction between the microbubble and the surrounding liquid is:

$$Re = \frac{\rho \omega R_0^2}{\mu} \gg 1, \;\; \mu < \frac{\mu_s}{R_0}$$

where ρ is the liquid density, μ and μ_s are the surrounding liquid viscosity and the shell viscosity respectively, ω is the forcing frequency and R_0 is the radius of the microbubble at equilibrium. The flow is assumed to be incompressible.

The surface of the bubble is described via spherical coordinates with r denoting the distance from the center of the bubble, $\tilde{r} = R_0 F(\theta)$ where $F(\theta, t)$ is the dimensionless radial position of the interface between the membrane and the surrounding liquid. The surface tension σ is used for the nondimensionalization of the pressure inside the bubble, $P = \tilde{P} / (2\sigma / R_0)$. The normal vector on the interface n is expressed through the unit vectors in spherical coordinates e_r, e_θ:

$$n = \frac{(F e_r - F_\theta e_\theta)^{\frac{1}{2}}}{F^2 + F_\theta^2} = n_r e_r + n_\theta e_\theta$$

where $F_\theta = \partial F / \partial \theta$.

The dimensionless equations and boundary conditions that describe the dynamic response of the microbubble are:

$$\nabla^2 \varphi = 0 \quad (0 \le r \le F(\theta), 0 \le \theta \le \pi) \tag{1}$$

$$\rho \frac{\partial \varphi}{\partial t} + \frac{\rho}{2} |\nabla \varphi|^2 + P = P_\infty \quad (0 \le r \le F(\theta), 0 \le \theta \le \pi) \tag{2}$$

$$\frac{\partial F}{\partial t} = \frac{\partial \varphi}{\partial r}\left(1 + \frac{F_\theta^2}{F^2}\right)^{1/2} \quad (r = F(\theta), 0 \le \theta \le \pi) \tag{3}$$

$$P_G - P_L = 2K_m\sigma + \Delta F_N \quad (r = F(\theta), 0 \le \theta \le \pi) \tag{4}$$

$$\Delta F_T = 0 \tag{5}$$

$$P = P_\infty, u \to 0, \quad z \to \pm\infty \tag{6}$$

The Laplace Equation (1) and the Bernoulli equation (2) describe the pressure and the velocity around the microbubble. The kinematic equation (3) is applied on the interface of the microbubble and correlates the velocity with the shape of the surface. The normal and tangential force equilibria (4,5) equalize the pressure difference of the interior and exterior of the microbubble with the surface tension and the residual viscoelastic tensions that are induced from the shell. The eq. (6) shows the assumption that the host liquid far away from the microbubble remains at a constant pressure.

2.1.1. Stability Analysis For Small Axisymmetric Disturbances

The Stability Analysis of the microbubble separates into two problems, depending on their order. We're mainly concerned about the zeroth and linear order problems and their respective equations.

To zeroth order, we have [2]:

$$R\ddot{R} + \frac{3}{2}\dot{R} = P_G(t) - \frac{2k_m^0}{We} - \Delta F_N^0 - P_\infty(t) \tag{7}$$

The equation presented above gives the instantaneous radial position of the surface of the microbubble, neglecting any perturbations of the system, where P_G is the pressure inside the bubble, $\Delta F^0{}_N$ the normal component of the elastic stresses on the shell at equilibrium, k_m^0 the average curvature of the bubble and We is the Weber number.

The initial state of the system at equilibrium is:

$$r = R_0$$

$$V = \overrightarrow{V_0} = 0$$

$$P_L = P_{st} = P_a \tag{8}$$

$$P_G = P_a + \frac{2\sigma}{R_0} + T_{el}$$

where in the last equation, it is shown that the pressure of the encapsulated gas is determined by the pressure of the surrounding liquid and the surface tension, by having the residual elastic stresses T_{el} being zero.

The equations that describe a perturbating system are derived from the oscillations of quantities circling the values given above, according to the oscillations' theory, as follows:

$$r = R_0 + \varepsilon w_1, \quad \theta = \theta_0 + \varepsilon u_1$$

$$\vec{V} = \overrightarrow{V_0} + \varepsilon\overrightarrow{V_1} = \varepsilon\vec{\nabla}\phi$$

$$P_L = P_\alpha + \varepsilon P_1 \tag{9}$$

$$P_G = \left(P_a + \frac{2\sigma}{R_0}\right) + \varepsilon P_{G,1}$$

Since $\overrightarrow{V_1} = \vec{\nabla}\phi$, the initial velocity and the the residual elastic stresses T_{el} equal zero. Where $w(\theta_0)$, $u(\theta_0)$ are the radial and azimuthal displacements of the microbubble's surface and ε is the magnitude of perturbation. Eq. (3) can be rewritten for the continuity of the normal velocity in the linear region and Eq. (4) as follows:

$$\frac{\partial w^1}{\partial t} = \frac{\partial \varphi^1}{\partial r} + \frac{\partial^2 \varphi_0}{\partial r^2}\bigg|_{r=R} w^1$$

$$P_G^1 - P_L^1 = 2K_m^1\sigma + \Delta F_N^1$$

At the same time the encapsulated gas oscillates approximately isothermally. Considering from the Poisson equation for isothermal process, we have:

$$P_G V^\gamma = P_0 V_0^\gamma \Rightarrow P_G = P_0\left(\frac{V_0}{V}\right)^\gamma \Rightarrow P_G^0 + \epsilon P_G^1 = P_G^0 \frac{V_0^\gamma}{V_0^\gamma}\frac{1}{1 + \epsilon 3\gamma w_0^1/R_0}$$

$$\rightarrow P_G^1 = -\frac{3\gamma P_G^0 w_0^1}{R_0}$$

Where γ is the polytropic gas constant and has values $1 \leq \gamma \leq 1.4$, V is the instantaneous dimensionless volume of the microbubble and V_0 is the initial volume of the microbubble, and since the bubble is spherical: $V_0 = \frac{4}{3}\pi$ (dimensionless). For an adiabatic process of the internal gas, γ=1.4 and for an isothermal process γ=1 instead.

For the second term of the Bernoulli equation between a particle of liquid near the microbubble and another in the far field, for the initially quiescent liquid we have:

$$\rho\frac{\partial \varphi_1}{\partial t} + P_L^1 = 0$$

While considering negligible pressure variations away from the microbubble.

To linear order and by ignoring compressibility and viscous effects on the surrounding liquid the equation of the normal force balance becomes:

$$-P_G - P^1|_{r=R} - \frac{\partial P^0}{\partial r}|_{r=R} w = \frac{2k_m^1}{w_e} + \Delta F_N^1 \quad (10)$$

In the following Φ is the Velocity potential of the velocity to linear order, R is the microbubble radius, $\dot{R}$ is the membrane velocity, $\ddot{R}$ is the membrane acceleration and w_n is the radial displacement of the membrane. We proceed the analysis by expanding each term of eq. (10)

By utilizing the Momentum equilibrium we obtain:

$$-P^1|_{r=R} = \sum_{n=1}^{\infty} P_n[\frac{\dot{\Phi}_n}{r^{n+1}} - \frac{\Phi_n(n+1)}{r^{n+4}}\dot{R}R^2] \Rightarrow$$

$$-P^1|_{r=R,n} = \frac{\dot{\Phi}_n(t)}{R^{n+1}} - \frac{\Phi_n(t)(n+1)}{R^{n+2}}\dot{R} \quad (11)$$

In the above we have implicitly introduced the expansions:

$$w^1 = \sum_{n=1}^{\infty} w_n(t) P_n(\theta), \quad \Phi^1 = \sum_{n=1}^{\infty} P_n(\theta)\frac{\Phi_n(t)}{r^{n+1}}, \quad P^1 = \sum_{n=1}^{\infty} P_n(\theta)\frac{p_n(t)}{r^{n+1}} \quad (11a)$$

where we neglect volume variations in order to study parametric shape mode excitation.
The second term of the Eq(4) becomes:

$$-\frac{\partial P^0}{\partial r}|_{r=R} w = \left[-\frac{2R\dot{R}^2+R^2\ddot{R}}{r^2} + \frac{4}{2}\frac{R^4\dot{R}^2}{r^5}|_{r=R}\right] w(-1) = \ddot{R}w \Rightarrow -\frac{\partial P^0}{\partial r}|_{r=R} w|_n = \ddot{R}w_n(t) \quad (12)$$

The third term of the Eq(4) becomes:

$$\frac{2k_m}{w_e} = -\frac{1}{w_e R^2}[H(w) + 2w] = -\frac{[H(w)+2w]}{w_e R^2} = \sum_{n=1}^{\infty} P_n(\theta)\frac{-[w_n - n(n+1)w_n]}{w_e R^2}$$

$$= \sum_{n=1}^{\infty} P_n(\theta) w_n(t)\frac{(n+2)(n-1)}{w_e R^2} \Rightarrow$$

for each Fourier component of the normal displacement of the membrane w:

$$\frac{2k_{m,n}}{w_e} = \frac{w_n(t)(n+2)(n-1)}{w_e R^2} \quad (13)$$

By utilizing the Kinematic Condition in the normal direction, we get:

$$\frac{\partial w}{\partial t} = V_r^1|_{r=R} + \frac{\partial V_r^0}{\partial r}|_{r=R} w - \frac{1}{r}\frac{\partial w}{\partial \theta} V_\theta^0|_{r=R} \Rightarrow \quad (14)$$

$$\Rightarrow \Phi^1 = \sum_{n=1}^{\infty} \frac{\Phi_n(t)}{r^{n+1}} P_r(\theta) \Rightarrow V_r^1 = \frac{\partial \Phi^1}{\partial r} = \sum_{n=1}^{\infty} \frac{\Phi_n(t)}{r^{n+2}}[-(n+1)]P_r(\theta) \quad (15)$$

$$V_r^0 = \frac{\partial \Phi^0}{\partial r} = \frac{\dot{R}R^2}{r^2}|_{r=R} \Rightarrow V_r^0|_{r=R} = \dot{R}$$

$$\frac{\partial V_r^0}{\partial r} = (-2)\frac{\dot{R}R^2}{r^3} \Rightarrow \frac{\partial V_r^0}{\partial r}|_{r=R} = -\frac{2\dot{R}}{R} \quad (16)$$

Upon substitution in eq. (14) it is obtained:

$$\frac{\partial w_n}{\partial t} = -\frac{\Phi_n(t)(n+1)}{R^{n+2}} - \frac{2\dot{R}}{R}w_n \Rightarrow \Phi_n(t) = -\dot{w}_n\frac{R^{n+2}}{n+1} - \frac{w_n R^{n+1}2\dot{R}}{n+1} \Rightarrow \quad (17)$$

$$\Rightarrow \dot{\Phi}_n(t) = -\ddot{w}_n\frac{R^{n+2}}{n+1} - \dot{w}_n\frac{n+2}{n+1}R^{n+1}\dot{R} - \dot{w}_n\frac{R^{n+1}2\dot{R}}{n+1} - \frac{w_n}{n+1}2[\ddot{R}R^{n+1} + (n+1)R^n\dot{R}^2] \Rightarrow$$

$$\Rightarrow \dot{\Phi}_n(t) = -\ddot{w}_n\frac{R^{n+2}}{n+1} - \dot{w}_n R^{n+1}\dot{R}\frac{n+4}{n+1} - \frac{2w_n R^n}{n+1}[\ddot{R}R + (n+1)\dot{R}^2] \quad (18)$$

By substituting the terms expanded above (12,13,14,15,16,17) and (18) in Eq (10) describing the normal force balance and modifying for the n-th eigenmode, we obtain:

$$-\ddot{w}_n\frac{R}{n+1} - \dot{w}_n\dot{R}\frac{n+4}{n+1} - \frac{2w_n}{(n+1)R}\left[\ddot{R}R + (n+1)\dot{R}^2\right] + \dot{w}_n\dot{R} + \dot{w}_n\frac{2\dot{R}^2}{R} + \dot{w}_n\ddot{R} =$$

$$= \frac{w_n}{w_e R^2}(n+2)(n-1) + \Delta F_{n,n}^{(1)} \Rightarrow$$

$$\ddot{w}_n + \dot{w}_n\frac{3\dot{R}}{R} + w_n\left[\frac{(n+1)(n+2)(n-1)}{w_e R^3} + \frac{\ddot{R}R + (n+1)\dot{R}^2}{R^2} - 2(n+1)\frac{\dot{R}^2}{R^2} - (n+1)\frac{\ddot{R}}{R}\right] +$$

$$+\Delta F_{n,n}^{(1)}\frac{(n+1)}{R} = 0 \Rightarrow$$

$$\ddot{w}_n + \dot{w}_n\frac{3\dot{R}}{R} + w_n\left[\frac{(n+1)(n+2)(n-1)}{w_e R^3} + (1-n)\frac{\ddot{R}}{R}\right] + \Delta F_{n,n}^{(1)}\frac{(n+1)}{R} = 0 \quad (19)$$

Which is the equation employed by Tsiglifis [2].
In order to complete the analysis of Eq (12) there is a need to examine the force balance in the normal direction. The Normal force balance consists of elastic and viscous components:

$$\Delta F_n^{(1)} = Elastic\ Stresses + Viscous\ Stresses = \Delta F_{n,el}^{(1)} + \Delta F_{n,v}^{(1)} \Rightarrow$$

$$\Rightarrow \Delta F_{n,n}^{(1)} = \Delta F_{n,el,n}^{(1)} + \Delta F_{n,v,n}^{(1)}$$

$$\Delta F_n^1 = \left[\kappa_s {\tau_{ss}}^v + \kappa_\varphi {\tau_{\varphi\varphi}}^v + \kappa_s {\tau_{ss}}^{el} + \kappa_\varphi {\tau_{\varphi\varphi}}^{el} - \frac{1}{\sigma}\frac{d}{ds}(\sigma q)\right]^1 \quad (20)$$

In order to calculate the normal force balance we need to first calculate the elastic stresses and the viscous stresses τ_{ss}^{el}, $\tau_{\varphi\varphi}^{el}$ and τ_{ss}^{v}, $\tau_{\varphi\varphi}^{v}$ respectively.

2.1.2. Elastic Stresses for Neo-Hookean Shell

Initiating the analysis for the elastic stresses in the Neo-Hookean type of shell:

$$\tau_{ss}{}^{el} = \frac{\chi[(\lambda_s^2-1)+v(\lambda_\varphi^2-1)]}{2(1-v^2)\lambda_\varphi} \quad (21)$$

$$\tau_{\varphi\varphi}{}^{el} = \frac{\chi[(\lambda_\varphi^2-1)+v(\lambda_s^2-1)]}{2(1-v^2)\lambda_s} \quad (22)$$

Where χ is a dimensionless number, $\lambda_s = R + \varepsilon(w + u_\theta)$ and $\lambda_\varphi = R + \varepsilon(w + u cot\theta_0)$

Regarding the λ_s and λ_φ variables we have:

$$\lambda_s = \frac{dS}{dS_0} = \frac{\sqrt{r^2\theta_\xi^2 + r_\xi^2}}{R_0\theta_{0\xi}} = \sqrt{r^2 + r_{\theta 0}^2}\,\frac{\theta_\xi}{R_0\theta_{0\xi}}$$

where $\theta_0=\pi\xi$, $r = R + \varepsilon w(\xi, t)$, $\theta \equiv \theta_0 + \varepsilon\frac{u(\xi,t)}{R}$

By differentiating each of the coordinates r,θ with the Lagrangian variable ξ we get:

$$\theta_\xi = \pi + \varepsilon\frac{u_\xi}{R},\ r_\xi = \varepsilon w_\xi$$

By raising λ_s, r_ξ and θ_ξ to the second power and executing the calculations in dimensionless form:

$$\lambda_s^2 = R^2\left[1 + \frac{2\varepsilon w}{R} + \cdots\right] \ , r_\xi^2 \cong O(\varepsilon^2)\ ,\ \theta_\xi^2 = (\pi + \frac{\varepsilon u_\xi}{R})^2 = \pi^2(1 + \frac{2\varepsilon u_\xi}{R\pi})$$

$$\lambda_s = \frac{\sqrt{R^2\left(1+\frac{2\varepsilon w}{R}+\cdots\right)\pi^2\left(1+\frac{2\varepsilon u_\xi}{R\pi}\right)+O(\varepsilon^2)}}{R_0\pi} \Rightarrow$$

$$\lambda_s = R + \varepsilon[w + u_\theta] \quad (23)$$

By working in a similar manner for λ_φ it is obtained:

$$\lambda_\varphi = \frac{rsin\theta}{R_0 sin\theta_0} = \frac{R\left(1 + \varepsilon\frac{w}{R}\right)\sin(\theta_0 + \varepsilon\frac{w}{R} + \cdots)}{R_0 sin\theta_0} \Rightarrow$$

$$\lambda_\varphi = \frac{R\left(1 + \varepsilon\frac{w}{R} + \cdots\right)[\sin\theta_0 + \varepsilon\frac{u}{R}cos\,\theta_0 + \cdots]}{R_0 sin\theta_0} \Rightarrow$$

$$\lambda_\varphi = R + \varepsilon[w + cot\theta_0 u] \quad (24)$$

By applying λ_s and λ_φ in the tension equations and expanding it, it is received:

$$\tau_{ss}{}^{el} = \frac{\chi}{2(1-v^2)}\frac{\left[R^2\left[1 + 2\varepsilon\left(\frac{w+u_\theta}{R}\right)\right] + vR^2\left[1 + 2\varepsilon\frac{w+cot\theta_0 u}{R}\right] - (1+v)\right]}{R + \varepsilon(w + cot\theta_0 u)} \Rightarrow$$

$$\Rightarrow {\tau_{ss}}^{el} = \frac{\chi(R^2-1)}{2(1-v)R} + \varepsilon\frac{\chi}{2R(1-v^2)}\Big[(2w + 2u_\theta + 2vw + v2ucot\theta_0)R - \frac{(w+cot\theta_0 u)}{R}(1 + v)(R^2-1)\Big]$$

And finally,

$${\tau_{ss}}^{el} = \frac{\chi(R^2-1)}{2(1-v)R} + \frac{\varepsilon\chi}{2R(1-v^2)}\{[2(w+u_\theta) + 2v(w+ucot\theta_0)]R -$$

$$-(1+v)\frac{(R^2-1)}{R}(w+ucot\theta_0)\} \quad (25)$$

By working similarly for the $\tau_{\varphi\varphi}$ tension equation we receive:

$${\tau_{\varphi\varphi}}^{el} = \frac{\chi}{2(1-v^2)}\frac{\left[R^2\left[1+2\varepsilon\frac{w+cot\theta_0 u}{R}\right] - 1 + vR^2\left[1+2\varepsilon\frac{w+u_\theta}{R} - v\right]\right]}{R\left[1+\varepsilon\frac{w+u_\theta}{R}\right]} \Rightarrow$$

$$\Rightarrow {\tau_{\varphi\varphi}}^{el} = \frac{(R^2-1)(1+v)\chi}{2R(1-v^2)} + \varepsilon\frac{\chi}{2(1-v^2)R}\Big\{R[2(w+ucot\theta_0) + 2v(w+u_\theta)] - (w+u_\theta)(1 + v)\frac{(R^2-1)}{R}\Big\} \quad (26)$$

2.1.3. Viscous Stresses for Neo-Hookean Shell

Next we have to evaluate the viscous stresses where both the dilatational and shear viscosities are considered.

$$\tau_{ss}^V = \left(\frac{1}{Re_s} + \frac{1}{Re_{shear}}\right) * \frac{S_{\xi,t}}{S_\xi} + \left(\frac{1}{Re_s} - \frac{1}{Re_{shear}}\right) * \frac{\sigma_t}{\sigma}$$

$$\tau_{\varphi\varphi}^V = \left(\frac{1}{Re_s} + \frac{1}{Re_{shear}}\right) * \frac{\sigma_t}{\sigma} + \left(\frac{1}{Re_s} - \frac{1}{Re_{shear}}\right) * \frac{S_{\xi,t}}{S_\xi}$$

As for S_ξ:

$$S_\xi = \sqrt{R^2\left[1+\varepsilon\frac{2w}{R} + \cdots\right]\pi^2\left(1+\varepsilon\frac{2u_\xi}{\pi R}\right) + O(\varepsilon^2)} \Rightarrow$$

$$S_\xi = R\pi\sqrt{1+\varepsilon\left(\frac{2w}{R} + \frac{2u_\xi}{R\pi}\right) + \cdots} \Rightarrow$$

In dimensionless form: $S_\xi = \pi[R + \varepsilon(w+u_\theta)] + \cdots O(\varepsilon^2)$ (27)

From Tsiglifis & Pelekasis [2] we have that: $\frac{S_{\xi,t}}{S_\xi} = \frac{1}{\lambda_s}\frac{\partial\lambda_s}{\partial t}$ and $\frac{\sigma_t}{\sigma} = \frac{1}{\lambda_\varphi}\frac{\partial\lambda_\varphi}{\partial t}$

By expanding the last two terms it is obtained:

$$\frac{S_{\xi,t}}{S_\xi}=\frac{1}{\lambda_s}\frac{\partial\lambda_s}{\partial t}=\frac{1}{R+\varepsilon(w+u_\theta)}\frac{\partial}{\partial t}[R+\varepsilon(w+u_\theta)]$$

$$\frac{\sigma_t}{\sigma}=\frac{1}{\lambda_\varphi}\frac{\partial\lambda_\varphi}{\partial t}=\frac{1}{R+\varepsilon(w+ucot\theta_0)}\frac{\partial}{\partial t}[R+\varepsilon(w+ucot\theta_0)]$$

$$\frac{S_{\xi,t}}{S_\xi}=\frac{\dot{R}+\varepsilon(\dot{w}+\dot{u}_\theta)}{R[1+\varepsilon\frac{w+u_\theta}{R}]}=\left(\frac{\dot{R}}{R}+\varepsilon\frac{\dot{w}+\dot{u}_\theta}{R}\right)\left[1-\varepsilon\frac{w+u_\theta}{R}\right]=$$

$$=\frac{\dot{R}}{R}+\varepsilon\left[\frac{\dot{w}+\dot{u}_\theta}{R}-\frac{\dot{R}}{R^2}(w+u_\theta)\right]+O(\varepsilon^2) \tag{28}$$

$$\frac{\sigma_t}{\sigma}=\left[\frac{\dot{R}}{R}+\varepsilon\left(\frac{\dot{w}}{R}+\frac{\dot{u}}{R}cot\theta_0\right)\right]\left[1-\varepsilon\frac{w+ucot\theta_0}{R}\right]=$$

$$=\frac{\dot{R}}{R}+\varepsilon\left[\frac{\dot{w}+\dot{u}cot\theta_0}{R}-\frac{\dot{R}}{R^2}(w+ucot\theta_0)\right]+O(\varepsilon^2) \tag{29}$$

Following this, by substituting the expanded expressions (22),(23) in the viscous stresses τ_{ss}^{v} and $\tau_{\varphi\varphi}^{v}$, we get:

$$\tau_{ss}^{V}=\frac{2}{Re_s}\frac{\dot{R}}{R}+\varepsilon\{\left(\frac{1}{Re_s}+\frac{1}{Re_{shear}}\right)\left[\frac{\dot{w}+\dot{u}_\theta}{R}-\frac{\dot{R}}{R^2}(w+u_\theta)\right]+$$

$$+\left[\frac{1}{Re_s}-\frac{1}{Re_{shear}}\right][\frac{\dot{w}+\dot{u}cot\theta_0}{R}-\frac{\dot{R}}{R^2}(w+ucot\theta_0)]\} \tag{30}$$

$$\tau_{\varphi\varphi}^{V}=\frac{2}{Re_s}\frac{\dot{R}}{R}+\varepsilon\{\left(\frac{1}{Re_s}+\frac{1}{Re_{shear}}\right)\left[\frac{\dot{w}+\dot{u}cot\theta_0}{R}-\frac{\dot{R}}{R^2}(w+ucot\theta_0)\right]+$$

$$+\left[\frac{1}{Re_s}-\frac{1}{Re_{shear}}\right][\frac{\dot{w}+\dot{u}_\theta}{R}-\frac{\dot{R}}{R^2}(w+u_\theta)]\} \tag{31}$$

Consequently the contribution of the viscous terms to the linear problem assumes the following form to linear order:

$$(\kappa_s\tau_{ss,v}+\kappa_\varphi\tau_{\varphi\varphi,v})^1=\left(\frac{1}{R}-\varepsilon\frac{w_{\theta\theta}+w}{R^2}\right)\left(\frac{2}{Re_s}\frac{\dot{R}}{R}+\varepsilon\left\{\left(\frac{1}{Re_s}+\frac{1}{Re_{shear}}\right)\left[\frac{\dot{w}+\dot{u}_\theta}{R}-\frac{\dot{R}}{R^2}(w+u_\theta)\right]+\right.\right.$$
$$\left.\left.\left[\frac{1}{Re_s}-\frac{1}{Re_{shear}}\right]\left[\frac{\dot{w}+\dot{u}cot\theta_0}{R}-\frac{\dot{R}}{R^2}(w+ucot\theta_0)\right]\right\}\right)+$$

$$+\left(\frac{1}{R}-\varepsilon\frac{w+w_\theta cot\theta_0}{R^2}\right)\left(\frac{2}{Re_s}\frac{\dot{R}}{R}+\varepsilon\left\{\left(\frac{1}{Re_s}+\frac{1}{Re_{shear}}\right)\left[\frac{\dot{w}+\dot{u}cot\theta_0}{R}-\frac{\dot{R}}{R^2}(w+ucot\theta_0)\right]+\right.\right.$$
$$\left.\left.+\left[\frac{1}{Re_s}-\frac{1}{Re_{shear}}\right]\left[\frac{\dot{w}+\dot{u}_\theta}{R}-\frac{\dot{R}}{R^2}(w+u_\theta)\right]\right\}\right)=$$

$$=\frac{4}{Re_s}\frac{\dot{R}}{R^2}+\varepsilon\{-\frac{2}{Re_s}\frac{\dot{R}}{R^3}(w_{\theta\theta}+w)-\frac{2}{Re_s}\frac{\dot{R}}{R^3}(w+w_\theta cot\theta_0)+$$

$$+\left[\frac{1}{Re_s}+\frac{1}{Re_{shear}}\right]\left[\frac{\dot{w}+\dot{u}_\theta}{R^2}-\frac{\dot{R}}{R^3}(w+u_\theta)+\frac{\dot{w}+\dot{u}cot\theta_0}{R^2}-\frac{\dot{R}}{R^3}(w+ucot\theta_0)\right]+$$

$$+\left[\frac{1}{Re_s}-\frac{1}{Re_{shear}}\right]\left[\frac{\dot{w}+\dot{u}cot\theta_0}{R^2}-\frac{\dot{R}}{R^3}(w+ucot\theta_0)+\frac{\dot{w}+\dot{u}_\theta}{R^2}-\frac{\dot{R}}{R^3}(w+u_\theta)\right]\} \tag{32}$$

Solving the above Equation (32) for the n-th eigenmode, we obtain:

$$(\kappa_s\tau_{ss,v} + \kappa_\varphi\tau_{\varphi\varphi,v})_n^1 =$$
$$-\frac{2}{Re_s}\frac{\dot{R}}{R^3}[2w_n - n(n+1)w_n] - \left[\frac{1}{Re_s} + \frac{1}{Re_{shear}} + \frac{1}{Re_s} - \frac{1}{Re_{shear}}\right]\frac{\dot{R}}{R^3}(2w + \Psi_{\theta\theta} + \Psi_\theta cot\theta) +$$
$$\left[\frac{1}{Re_s} + \frac{1}{Re_{shear}} + \frac{1}{Re_s} - \frac{1}{Re_{shear}}\right]\frac{1}{R^2}\left(2\dot{w} + \dot{\Psi}_{\theta\theta} + \dot{\Psi}_\theta cot\theta\right) =$$

$$= -\frac{2}{Re_s}[4w_n - n(n+1)w_n - n(n+1)\Psi_n]\frac{\dot{R}}{R^3} + \frac{2}{Re_s}\frac{1}{R^2}[2\dot{w} - n(n+1)\dot{\Psi}_n] \quad (33)$$

Where: $u \equiv \frac{\partial\Psi}{\partial\theta}$, u being the displacement in the azimuthal direction.

κ_φ and κ_s are calculated in dimensionless form:

$$\kappa_\varphi = \frac{\theta_\xi}{S_\xi} - \frac{r_\xi cot\theta}{S_\xi r} \Rightarrow$$

$$\kappa_\varphi = \frac{\pi(1 + \varepsilon\frac{u_\theta}{R})}{\pi[R + \varepsilon(w + u_\theta)]} - \frac{\varepsilon w_\xi(cot\theta_0 - \varepsilon\frac{u}{R}\frac{1}{sin^2\theta_0})}{\pi[R + \varepsilon(w + u_\theta)][R + \varepsilon w]} \Rightarrow$$

$$\Rightarrow \kappa_\varphi = \frac{1}{R} - \varepsilon\left[\frac{w}{R^2} + \frac{w_\theta cot\theta_0}{R^2}\right] + O(\varepsilon^2) \quad (34)$$

$$\kappa_s = \frac{r_\xi^2\theta_\xi}{S_\xi^3} + \frac{rr_\xi\theta_{\xi\xi} - rr_{\xi\xi}\theta_\xi}{S_\xi^3} + \frac{\theta_\xi}{S_\xi} \Rightarrow$$

$$\Rightarrow \kappa_s = -\frac{\varepsilon}{\pi^2R^2}w_{\xi\xi} + \frac{1}{R}\left[1 + \varepsilon\left(\frac{u_\theta}{R} - \frac{w+u_\theta}{R}\right)\right] \Rightarrow \kappa_s^1 = \frac{1}{R} - \varepsilon\frac{w_{\theta\theta}+w}{R^2} \quad (35)$$

$$\frac{\kappa_s + \kappa_\varphi}{2} = \left[\frac{2}{R} + \varepsilon\left[-\frac{w_{\theta\theta}}{R^2} - \frac{2w}{R^2} - \frac{w_\theta cot\theta_0}{R^2}\right]\right]\frac{1}{2} \Rightarrow$$

$$\Rightarrow \kappa_m = \frac{1}{R} - \varepsilon\left[\frac{w_{\theta\theta}}{2R^2} + \frac{w}{R^2} + \frac{w_\theta cot\theta_0}{2R^2}\right] \quad (36)$$

Where κ_s, κ_φ are the two principal curvatures and κ_m is the mean curvature.

2.1.4. Bending Stresses for Neo-Hookean Shell

Moving on to the next part, the bending stresses [2] are processed:

$$\tau_{b,n} = \frac{1}{\rho}\frac{\partial}{\partial s}(\rho q) = \frac{\partial q}{\partial s} + \frac{q}{\rho}\frac{\partial\rho}{\partial s} \quad (37)$$

$$q = \frac{1}{\rho}\frac{\partial\rho}{\partial s}[\frac{\partial}{\partial\rho}(\rho m_s) - m_\varphi] \quad (38)$$

$$m_s = \frac{\kappa_B}{\lambda_\varphi}(K_s + v_s K_\varphi)\ ,\ m_\varphi = \frac{\kappa_B}{\lambda_s}(K_\varphi + v_s K_s) \quad (39)$$

$$K_s = \lambda_s\kappa_s - \kappa_s^R\ ,\ K_\varphi = \lambda_\varphi\kappa_\varphi - \kappa_\varphi^R \quad (40)$$

Where m_s, m_φ, are the bending moments manifesting on the membrane, $\tau_{b,n}$ is the bending stress and q vectorial transverse shear tension. Also κ_s^R, κ_φ^R are the dimensionless reference curvatures in the principal directions.

K_s and K_φ are the bending measures of strain as introduced by [1]

By replacing the expanded terms on the equations (31-34) we get:

$$K_s = R\left[1+\varepsilon\frac{w+u_\theta}{R}\right]\left[\frac{1}{R}-\varepsilon\frac{w_{\theta\theta}+w}{R^2}\right]-1 \Rightarrow$$

$$\Rightarrow K_s = \varepsilon\left(\frac{w+u_\theta}{R}-\frac{w_{\theta\theta}+w}{R}\right)=\varepsilon\frac{u_\theta-w_{\theta\theta}}{R} \tag{41}$$

$$K_\varphi = R\left[1+\varepsilon\frac{w+ucot\theta_0}{R}\right]\left[\frac{1}{R}-\varepsilon\frac{w+w_\theta cot\theta_0}{R^2}\right]-1 \Rightarrow$$

$$\Rightarrow K_\varphi = \varepsilon\frac{w+ucot\theta_0-w-w_\theta cot\theta_0}{R}=\varepsilon\frac{cot\theta_0[u-w_\theta]}{R} \tag{42}$$

$$m_s = \frac{\kappa_B}{R}\varepsilon\left[\frac{u_\theta-w_{\theta\theta}}{R}+v_s\frac{cot\theta_0[u-w_\theta]}{R}\right]=\varepsilon\frac{\kappa_B}{R^2}[u_\theta-w_{\theta\theta}+v_s cot\theta_0(u-w_\theta)] \tag{43}$$

$$m_\varphi = \frac{\kappa_B}{R^2}\varepsilon[cot\theta_0(u-w_\theta)+v_s(u_\theta-w_{\theta\theta})] \tag{44}$$

$$q = \frac{1}{\rho}\frac{\partial\rho}{\partial s}\left[m_s-m_\varphi+\rho\frac{\partial m_s}{\partial\rho}\right]=\frac{m_s-m_\varphi}{\rho}\frac{\partial\rho}{\partial s}+\frac{\partial m_s}{\partial s} \tag{45}$$

where: $\frac{\partial m_s}{\partial s}=\frac{\frac{\partial m_s}{\partial\xi}}{\frac{\partial s}{\partial\xi}}$

Also:

$$\rho = rsin\theta \Rightarrow \rho = (R+\varepsilon w)(sin\theta_0+\frac{\varepsilon u}{R}cos\theta_0+\cdots)\Rightarrow$$

$$\Rightarrow \rho = Rsin\theta_0+\varepsilon[wsin\theta_0+ucos\theta_0]+O(\varepsilon^2)$$

$$\frac{\partial\rho}{\partial s}=\frac{\rho_\xi}{s_\xi}=\frac{r_\xi sin\theta+rcos\theta\theta_\xi}{\sqrt{r_\xi^2+r^2\theta_\xi^2}}$$

The contribution of the bending stresses in the tangential force balance is the following:

$$-k_s q = -\varepsilon\frac{k_B}{R^4}\{(1-v)cot\theta_0(u_\theta-w_{\theta\theta})-cot^2\theta_0(u-w_\theta)(1-v)+$$

$$+(u_{\theta\theta}-w_{\theta\theta\theta})+vcot\theta_0(u_\theta-w_{\theta\theta})+v(u-w_\theta)\frac{d}{d\theta}cot\theta_0\}=$$

$$=\varepsilon\frac{k_B}{R^4}\big(-\lambda_n+(1-v)\big)E=\frac{\varepsilon k_B}{R^4}[-\lambda_n+1-v](w_\theta-\Psi_\theta) \tag{46}$$

Where $E = w_\theta - \Psi_\theta$

By differentiating ρ with s we get:

$$\frac{\partial\rho}{\partial s}=\frac{\varepsilon w_\xi\left[sin\theta_0+\varepsilon\frac{u}{R}cos\theta_0+\cdots\right]+R\left(1+\varepsilon\frac{w}{R}\right)\pi\left(1+\varepsilon\frac{u_\xi}{\pi R}\right)\left(cos\theta_0-\frac{\varepsilon u}{R}sin\theta_0+\varepsilon^2\right)}{\pi R\left[1+\varepsilon\frac{w+u_\theta}{R}\right]}\Rightarrow$$

$$\Rightarrow\frac{\partial\rho}{\partial s}=cos\theta_0+\varepsilon cos\theta_0\frac{2u_\theta-utan\theta_0+w_\theta tan\theta_0}{R} \quad (47)$$

By doing further differentiations to various terms we receive the forms used in the aforementioned equations:

$$\frac{\partial m_s}{\partial\xi}=\varepsilon\frac{k_B}{R^2}\left[u_{\theta\xi}-w_{\theta\theta\xi}+v_s\frac{\partial cot\theta_0}{\partial\xi}(u-w_\theta)+v_s cot\theta_0\left(u_\xi-w_{\theta\xi}\right)\right]$$

$$\frac{ds}{d\xi}=\pi R\left[1+\varepsilon\frac{w+u_\theta}{R}\right]$$

Then by applying those terms to the equation of the transverse shear stresses (45) and by expanding we receive:

$$q=\varepsilon\left\{\frac{k_B}{R^3}cot\theta_0[(u_\theta-w_{\theta\theta})cot\theta_0(u-w_\theta)](1-v)+\frac{k_B}{R^3}\left[u_{\theta\theta}-w_{\theta\theta\theta}+v\frac{\partial cot\theta_0}{\partial\theta_0}(u-w_\theta)+vcot\theta_0(u_\theta-w_{\theta\theta})\right]\right\}\Rightarrow$$

$$\Rightarrow q=\varepsilon\frac{k_B}{R^3}\{cot\theta_0[(u_\theta-w_{\theta\theta})-cot\theta_0(u-w_\theta)](1-v)+$$

$$+[(u_{\theta\theta}-w_{\theta\theta\theta})+v\frac{\partial}{\partial\theta_0}[cot\theta_0(u-w_\theta)]]\}$$

So the bending stresses equation becomes:

$$-\tau_{B,n}=\frac{\varepsilon k_B}{R^4}\left\{cot\theta[-\lambda_n A_\theta+(1-v)A_\theta]+\frac{d}{d\theta}[-\lambda_\theta A_\theta+(1-v)A_\theta]\right\}\Rightarrow$$

$$-\tau_{B,n}=\frac{\varepsilon k_B}{R^4}\{(1-v)[A_{\theta\theta}+cot\theta A_\theta]+cot\theta\frac{d}{d\theta}[A_{\theta\theta}+cot\theta A_\theta]+$$
$$+\frac{d^2}{d\theta^2}(A_{\theta\theta}+cot\theta A_\theta)\} \quad (48)$$

Based on the identities noted in the appendix we have:

$$A=w-\Psi$$
$$A_{\theta\theta\theta}=A_\theta(-1+cot^2\theta)+cot\theta A_{\theta\theta}=\left[\frac{d^3}{d\theta^3}+cot\theta\frac{d^2}{d\theta^2}-(1+cot^2\theta)\frac{d}{d\theta}\right]A=$$

$$-\lambda_n\frac{d}{d\theta}A=-\lambda_n(w_\theta-\Psi_\theta) \quad (49)$$

2.1.5. Normal Force Balance on the Shell

Since both the elastic and the viscous stresses are evaluated, as well as the bending stresses and moments, we proceed with the expansion of the normal force balance:

$$\Delta F_{N,H}{}^{1} = -\frac{w_{\theta\theta}+w}{R^2}\frac{\chi(R^2-1)}{2(1-v)R} + \frac{\chi}{2R^2(1-v^2)}\Big\{R[2(w+u_\theta)+2v(w+ucot\theta)] - (1+ v)\frac{R^2-1}{R}(w+ucot\theta)\Big\} -$$

$$-\frac{w+w_\theta cot\theta}{R^2}\frac{\chi(R^2-1)}{2(1-v)R} + \frac{\chi}{2(1-v^2)R^2}\Big\{R[2(w+ucot\theta)+(w+u_\theta)2v] - (w+u_\theta)(1+ v)\frac{R^2-1}{R}\Big\} +$$

$$+\frac{2}{Re_s R^2}(2\dot{w}+\dot{u}_\theta+\dot{u}cot\theta) + \frac{\varepsilon k_B}{R^4}\big[\lambda_n(\lambda_n-(1-v))\big](w-\Psi) \Rightarrow$$

$$\Delta F_{N,H}{}^{1} = -\frac{\chi(R^2-1)}{2(1-v)R^3}(2w+w_{\theta\theta}+w_\theta cot\theta) +$$

$$+\frac{\chi}{2R^2(1-v^2)}\Big\{2R[(w+u_\theta)(1+v)+(w+ucot\theta)(1+v)] - (1+v)\frac{R^2-1}{R}(2w+u_{\theta\theta} - ucot\theta)\Big\} +$$

$$+\frac{2}{Re_s R^2}(2\dot{w}+\dot{u}_\theta+\dot{u}cot\theta) + \frac{k_B}{R^4}\big[\lambda_n(\lambda_n-(1-v))\big](w-\Psi) \Rightarrow$$

$$\Delta F_{N,H}{}^{1} = \frac{\chi}{2R^3(1-v)}[(2w+u_\theta+ucot\theta)(R^2+1) - (2w+w_{\theta\theta}+w_\theta cot\theta)(R^2-1)] +$$

$$+\frac{2}{Re_s R^2}(2\dot{w}+\dot{u}_\theta+\dot{u}cot\theta) + \frac{k_B}{R^4}\lambda_n[\lambda_n-(1-v)(w-\Psi)]$$

$$\Delta F_{N,H}{}^{1} = \frac{\chi}{2R^3(1-v)}[(R^2+1)(2w+u_\theta+ucot\theta) - (R^2-1)(2w+w_{\theta\theta}+w_\theta cot\theta)] +$$

$$+\frac{2}{Re_s R^2}\big(2\dot{w}-\lambda_n\dot{\Psi}\big) + \frac{k_B}{R^4}\big[\lambda_n{}^2-\lambda_n(1-v)\big](w-\Psi) \qquad (50)$$

2.1.6. Tangential Stress Balance on the Shell

The next equation that needs to be expanded to linear order including the viscous contribution is the tangential stress balance:

$$\frac{\partial\tau_{ss}}{\partial s} + \frac{1}{\sigma}\frac{\partial\sigma}{\partial s}\big(\tau_{ss}-\tau_{\varphi\varphi}\big) = \frac{\partial\tau_{ss}}{\partial\xi}\frac{\partial\xi}{\partial s} + \frac{1}{rsin\theta}\frac{\partial(rsin\theta)}{\partial\xi}\frac{\partial\xi}{\partial s}\big(\tau_{ss}-\tau_{\varphi\varphi}\big) =$$

$$= \frac{\partial\tau_{ss}}{\partial\theta_0}\frac{\partial\theta_0}{\partial s} + \frac{1}{rsin\theta}\frac{\partial(rsin\theta)}{\partial\theta_0}\frac{\partial\theta_0}{\partial s}\big(\tau_{ss}-\tau_{\varphi\varphi}\big) \qquad (51)$$

From Tsiglifis & Pelekasis [2] it is shown that:

$$\frac{\partial s}{\partial\xi} = \sqrt{r^2\theta_\xi^2+r_\xi^2} \Rightarrow \frac{\partial s}{\partial\theta_0}\frac{\partial\theta_0}{\partial\xi} = \sqrt{r^2\theta_{\theta_0}^2+r_{\theta_0}^2} \Rightarrow \frac{\partial s}{\partial\theta_0} = \sqrt{r^2\theta_{\theta_0}^2+r_{\theta_0}^2}$$

Plus, the cylindrical coordinates are given by the equations:

$$r = R+\varepsilon w \ , \qquad \theta = \theta_0+\frac{u}{R}\varepsilon \qquad (52)\ ,(53)$$

Where: *w*,u: displacements along the radial and azimuthal direction respectively

By differentiating the terms of the tangential stress balance equation with the initial angle θ_0, we get:

$$\frac{\partial r}{\partial \theta_0} = \varepsilon w_\theta \tag{54}$$

$$\frac{\partial \theta}{\partial \theta_0} = 1 + \frac{u_\theta}{R} \tag{55}$$

$$\frac{\partial s}{\partial \theta_0} = \sqrt{R^2\left[1 + 2\varepsilon\frac{w}{R} + O(\varepsilon^2)\right](1 + 2\frac{u_\theta}{R}\varepsilon + O(\varepsilon^3)) + O(\varepsilon^2)} \Rightarrow$$

$$\Rightarrow \frac{\partial s}{\partial \theta_0} = R\sqrt{1 + 2\left(\frac{w}{R} + \frac{u_\theta}{R}\right)\varepsilon + O(\varepsilon)} = R[\left(1 + \frac{w+u_\theta}{R} + \cdots\right)] \Rightarrow$$

$$\Rightarrow \frac{\partial \theta_0}{\partial s} = \frac{1}{R}[1 - \varepsilon\frac{w+u_\theta}{R} + \cdots] \tag{56}$$

$$\frac{\partial(rsin\theta)}{\partial \theta_0} = \frac{\partial r}{\partial \theta_0}sin\theta + r\frac{\partial sin\theta}{\partial \theta_0}$$

$$sin\theta = \sin\left(\theta_0 + \frac{u}{R}\varepsilon\right) = sin\theta_0 + cos\theta_0\frac{u}{R}\varepsilon + (\dots) \tag{57}$$

$$\frac{\partial sin\theta_0}{\partial \theta_0} = cos\theta_0 + \frac{\varepsilon}{R}(u_\theta cos\theta_0 - usin\theta_0)$$

$$rsin\theta = Rsin\theta_0 + \varepsilon[ucos\theta_0 + sin\theta_0 R] + (\dots) \tag{58}$$

$$\frac{\partial rsin\theta}{\partial \theta_0} = \varepsilon w_\theta sin\theta_0 + Rcos\theta_0 + \varepsilon[u_\theta cos\theta_0 - usin\theta_0] =$$

$$= Rcos\theta_0 + \varepsilon[w_\theta sin\theta_0 + u_\theta cos\theta_0 - usin\theta_0] \tag{59}$$

By utilizing the identities that appear in the appendix A, it is proven that:

$$\dot{\Psi}_{\theta\theta\theta} + \left(\dot{\Psi}_\theta cot\theta\right)_\theta = \left(\dot{\Psi}_{\theta\theta} + \dot{\Psi}_\theta cot\theta\right)_\theta = -n(n+1)\Psi_\theta$$

$$\dot{u}_{\theta\theta} + cot\theta(\dot{u}_\theta - \dot{u}cot\theta) = \dot{\Psi}_{\theta\theta} + cot\theta\dot{\Psi}_{\theta\theta} - \dot{\Psi}_\theta cot^2\theta =$$

$$= \dot{\Psi}_{\theta\theta\theta} + cot\theta\dot{\Psi}_{\theta\theta} - \dot{\Psi}_\theta cot^2\theta - \dot{\Psi}_\theta + \dot{\Psi}_\theta =$$

$$= \left[\dot{\Psi}_{\theta\theta} + cot\theta\dot{\Psi}_\theta\right]_\theta + \dot{\Psi}_\theta = -n(n+1)\dot{\Psi}_\theta + \dot{\Psi}_\theta =$$

$$= \dot{\Psi}_\theta[1 - n(n+1)]$$

Where: $u = \frac{\partial \Psi}{\partial \theta}$

It is also proven that:

$$\dot{u}_{\theta\theta} + (\dot{u}cot\theta_0)_\theta = \left(\dot{\Psi}_{\theta\theta} + \dot{\Psi}_\theta cot\theta\right)_\theta = -n(n+1)\Psi_\theta$$

By substituting the above expansions in the tangential stress balance and by simplifying it is obtained:

$$\frac{\partial \tau_{ss}}{\partial \theta_0}\frac{\partial \theta_0}{\partial s}+\frac{1}{rsin\theta}\frac{\partial (rsin\theta)}{\partial \theta_0}\frac{\partial \theta_0}{\partial s}\left(\tau_{ss}-\tau_{\varphi\varphi}\right)=$$

$$=\frac{1}{R}\left[1-\varepsilon\frac{w+u_\theta}{R}+\cdots\right]\varepsilon\{\left(\frac{1}{Re_s}+\frac{1}{Re_{shear}}\right)\left[\frac{\dot{w}_\theta+\dot{u}_{\theta\theta}}{R}-\frac{\dot{R}}{R^2}\left(w_\theta+u_{\theta\theta}\right)\right]+$$

$$+\left[\frac{1}{Re_s}-\frac{1}{Re_{shear}}\right]\left[\frac{\dot{w}_\theta+\dot{u}_\theta cot\theta_0+\dot{w}cot\dot{\theta}_0}{R}-\frac{\dot{R}}{R^2}\left(w_\theta+u_\theta cot\theta_0+ucot\dot{\theta}_0\right)\right]\}+$$

$$+\frac{1}{Rsin\theta_0}[1-\varepsilon(ucos\theta_0+Rsin\theta_0)]\frac{1}{R_0}\left[1-\varepsilon\frac{w+u_\theta}{R}+(\dots)\right]*$$

$$Rcos\theta_0\left[1+\varepsilon\left(\frac{w_\theta}{R}tan\theta_0+\frac{u_\theta}{R}-\frac{u}{R}tan\theta_0\right)\right]*$$

$$*\,\varepsilon[\left(\frac{1}{Re_s}+\frac{1}{Re_{shear}}\right)\left[\frac{\dot{u}_\theta-\dot{u}cot\theta_0}{R}+\frac{\dot{R}}{R^2}\left(ucot\theta_0-u_\theta\right)\right]+\left(\frac{1}{Re_s}-\frac{1}{Re_{shear}}\right)*$$

$$*\left[\frac{\dot{u}cot\theta_0-\dot{u}_\theta}{R}+\frac{\dot{R}}{R^2}\left(u_\theta-ucot\theta_0\right)\right]] \quad (60)$$

Thus, the final form of the tangential stress balance (51), when the dilatational and shear viscosities reads as:

$$\dot{\Psi}\left[\frac{n(n+1)}{R^2}\left(\frac{1}{Re_s}-\frac{1}{Re_{shear}}\right)-\frac{2}{R^2Re_{shear}}\left(1-n(n+1)\right)\right]=$$

$$=\frac{2}{R^3Re_s}\left(R\dot{w}-\dot{R}w\right)+\Psi\left[\frac{\dot{R}(n+1)n}{R^3}\left(\frac{1}{Re_s}-\frac{1}{Re_{shear}}\right)-\frac{2\dot{R}}{R^3Re}[1-n(n+1)]\right] \quad (61)$$

By moving the right hand side of the equation (61) to the left we have:

$$\dot{\Psi}\left[\frac{n(n+1)}{R^2}\left(\frac{1}{Re_s}-\frac{1}{Re_{shear}}\right)-\frac{2}{R^2Re_{shear}}\left(1-n(n+1)\right)\right]-\frac{2}{R^3Re_s}\left(R\dot{w}-\dot{R}w\right)-$$
$$\Psi\left[\frac{\dot{R}(n+1)n}{R^3}\left(\frac{1}{Re_s}-\frac{1}{Re_{shear}}\right)-\frac{2\dot{R}}{R^3Re}[1-n(n+1)]\right]=0 \quad (62)$$

2.1.7 Tangential Force Balance on the Shell

Additionally, the Tangential Force balance for the linear problem is calculated:

$$\Delta {F_T}^1=\left[-\frac{\partial {\tau_{ss}}^v}{\partial s}-\frac{1}{\sigma}\frac{\partial \sigma}{\partial s}\left({\tau_{ss}}^v-{\tau_{\varphi\varphi}}^v\right)-\frac{\partial {\tau_{ss}}^{el}}{\partial s}-\frac{1}{\sigma}\frac{\partial \sigma}{\partial s}\left({\tau_{ss}}^{el}-{\tau_{\varphi\varphi}}^{el}\right)-\kappa_s q\right]^1$$

By substituting the viscous and elastic stresses in the Tangential Force balance we have:

$$\Delta {F_{T,H}}^1=\frac{k_B}{R^4}[1-v-\lambda_n](w_\theta-\Psi_\theta)-\frac{cot\theta}{R}\frac{\chi}{2R(1-v^2)}\{(1+v)\frac{R^2-1}{R}[w+u_\theta-w-ucot\theta]+$$

$$+2R[(w+u_\theta)(1-v)+(w+ucot\theta)(v-1)]\}-\frac{\chi}{2R^2(1-v^2)}\{2R[w_\theta+u_{\theta\theta}+v[w_\theta+ucot\theta-u-ucot^2\theta]-$$

$$-(1+v)\frac{R^2+1}{R}(w_\theta+u_\theta cot\theta-u-ucot^2\theta)\}-\frac{2}{Re_s}\frac{\dot{w}_\theta+\dot{u}_{\theta\theta}}{R^2}-\frac{cot\theta}{R}\frac{2}{Re_sR}(\dot{w}+\dot{u}_\theta-\dot{w}-\dot{u}cot\theta)-$$

$$-\frac{2}{Re_sR^3}[-R\dot{w}_\theta-R(1-\lambda_n)\dot{\Psi}_\theta]\Rightarrow$$

$$\Delta F_{T,H}{}^1=\frac{k_B}{R^4}[1-v-\lambda_n](w_\theta-\Psi_\theta)-\frac{cot\theta\chi}{2R^2(1-v^2)}(u_\theta-ucot\theta)\left[(1+v)\frac{R^2-1}{R}+2R(1-v)\right]-$$

$$-\frac{\chi}{2R^2(1-v^2)}\{2R(w_\theta+u_{\theta\theta})+(w_\theta+u_\theta cot\theta-u-ucot^2\theta)\left[\frac{2R^2v-(1+v)(R^2-1)}{R}\right]\Rightarrow$$

$$\Delta F_{T,H}{}^1=\frac{k_B}{R^4}[1-v-\lambda_n](w_\theta-\Psi_\theta)-\frac{\chi}{2R^2(1-v^2)}\left[2R[w_\theta+u_{\theta\theta}+u_\theta cot\theta-ucot^2\theta]+(u-w_\theta)-\frac{R^2(1-v)-(1+v)}{R}\right]-$$

$$-\frac{2}{Re_sR^2}[\dot{w}_\theta+\dot{u}_{\theta\theta}+cot\theta\dot{u}_\theta-cot^2\theta\dot{u}]\Rightarrow$$

$$\Delta F_{T,H}{}^1=\frac{k_B}{R^4}[1-v-\lambda_n](w_\theta-\Psi_\theta)-\frac{\chi}{2R^2(1-v^2)}\left[2R[w_\theta+u_{\theta\theta}+u_\theta cot\theta-ucot^2\theta]+(u-w_\theta)-\frac{R^2(1-v)-(1+v)}{R}\right]-$$

$$-\frac{-2}{Re_sR^3}[-R\dot{w}_\theta+R(\dot{\Psi}_{\theta\theta\theta}+cot\theta\dot{\Psi}_{\theta\theta}-cot^2\theta\dot{\Psi}_\theta)\Rightarrow$$

$$\Delta F_{T,H}{}^1=-\frac{\chi}{2R^2(1-v^2)}\left\{2R[w_\theta+u_{\theta\theta}+u_\theta cot\theta-ucot^2\theta]+(u-w_\theta)\frac{R^2(1-v)-(1+v)}{R}\right\}+$$

$$+\frac{k_B}{R^4}(1-v-\lambda_n)(w_\theta-\Psi_\theta)-\frac{2}{Re_sR^3}\left[R\dot{w}_\theta+R(1-\lambda_n)\dot{\Psi}_\theta\right]\Rightarrow$$

$$\Delta F_{T,H}{}^1=\frac{k_B}{R^4}(1-v-\lambda_n)(w_\theta-\Psi_\theta)-\frac{2}{Re_sR^3}\left[R\dot{w}_\theta+R(1-\lambda_n)\dot{\Psi}_\theta\right]-$$

$$-\frac{\chi}{2R^2(1-v^2)}\left[2R[w_\theta+u_{\theta\theta}+u_\theta cot\theta-ucot^2\theta]+(u-w_\theta)\frac{R^2(1-v)-(1+v)}{R}\right]\Rightarrow$$

$$\Delta F_{T,H}{}^1=-\frac{\chi}{2R^3(1-v)}\left\{(R^2+1)w_\theta+\Psi_\theta\left[R^2\frac{2(1-\lambda_n)+1-v}{1+v}-1\right]\right\}+$$

$$+\frac{k_B}{R^4}(1-v-\lambda_n)(w_\theta-\Psi_\theta)-\frac{2}{Re_sR^2}\left[\dot{w}_\theta+(1-\lambda_n)\dot{\Psi}_\theta\right]\Rightarrow$$

$$\Delta F_{T,H}{}^1=\frac{k_B}{R^4}(1-v-\lambda_n)(w_\theta-\Psi_\theta)-\frac{2}{Re_sR^2}\left[\dot{w}_\theta+(1-\lambda_n)\dot{\Psi}_\theta\right]-$$

$$-\frac{\chi}{2R^3(1-v)}\left\{u\left[R^2\frac{2(1-\lambda_n)+1-v}{1+v}-1\right]+w_\theta(R^2+1)\right\}\Rightarrow$$

$$\Delta F_{T,H}{}^1=\frac{k_B}{R^4}(1-v-\lambda_n)(w_\theta-\Psi_\theta)-\frac{2}{Re_sR^3}\left[R\dot{w}_\theta+R(1-\lambda_n)\dot{\Psi}_\theta\right]-$$

$$-\frac{\chi}{2R^2(1-v^2)}\left[u\left[\frac{2R^2(1-\lambda_n)+R^2(1-v)-(1+v)}{R}\right]+w_\theta\left[\frac{2R^2+(1+v)-R^2(1-v)}{R}\right]\right] \quad (63)$$

By substituting eq. (62) to the viscous term of eq. (63) we obtain:

$$\Delta F_{T,H}{}^1=\frac{k_B}{R^4}(1-v-\lambda_n)(w_\theta-\Psi_\theta)-\dot{\Psi}\left[\frac{n(n+1)}{R^2}\left(\frac{1}{Re_s}-\frac{1}{Re_{shear}}\right)-\frac{2}{R^2Re_{shear}}\left(1-n(n+1)\right)\right]+\frac{2}{R^3Re_s}\left(R\dot{w}-\dot{R}w\right)+\Psi\left[\frac{\dot{R}(n+1)n}{R^3}\left(\frac{1}{Re_s}-\frac{1}{Re_{shear}}\right)-\frac{2\dot{R}}{R^3Re}[1-n(n+1)]\right]-$$

$$-\frac{\chi}{2R^2(1-v^2)}\left[u\left[\frac{2R^2(1-\lambda_n)+R^2(1-v)-(1+v)}{R}\right]+w_\theta\left[\frac{2R^2+(1+v)-R^2(1-v)}{R}\right]\right] \quad (64)$$

which shows the contribution of the shear viscosity to the tangential force balance.

2.1.8. Stability Analysis to Non-Spherical Disturbances

In this section the manner in which the equations that pertain to the stability analysis are affected is shown, and the relevant analysis is conducted.

By letting $w_n=a_ne^{\omega_nt}$, $\Psi_n=B_ne^{\omega_nt}$ and by substituting the terms in the normal and tangential force balance equations (19) and (61) we obtain:

$$\ddot{w}_n+\frac{3\dot{R}}{R}\dot{w}_n+[(1-n)\frac{\ddot{R}}{R}+\frac{(n+1)(n-1)(n+2)}{W_eR^3}]w_n+\frac{(n+1)}{R}\Delta F_n^1=0 \quad (65)$$

$$\Delta F_t^1=0 \quad (66)$$

Upon carrying out the calculations, the resulting equations for the normal force balance:

$$\omega_n{}^2a_n+\frac{(n+1)(n-1)(n+2)}{W_eR^3}a_n+\frac{(n+1)}{R}\left(-\frac{1}{3R^8}\right)\{-\lambda_na_n[R^6-1]-\lambda_nB_n(-6)+a_n[2R^6-14]\}+\frac{(n+1)}{R}\frac{2}{Re_sR^3}*$$

$$*\left[-R\lambda_nB_n\omega_n+2R\omega_na_n\right]+\ +\frac{n+1}{R}\frac{B}{R^4}[\lambda_n^2(a_n-B_n)+(1-v)\lambda_n(B_n-a_n)]=0 \quad (67)$$

and the equivalent equation for the tangential force balance assume the form:

$$-\frac{1}{3R^8}\{a_n(6)+B_n(2R^6-3\lambda_n-R^6\lambda_n)\}+$$

$$+\frac{2}{Re_sR^3}[-R(1-\lambda_n)B_n\omega_n-R\omega_na_n]+\frac{B}{R^4}(a_n-B_n)(1-v-\lambda_n)=0 \quad (68)$$

Then we proceed by extracting the terms a_n and B_n as common factors and by allowing R to be equal to 1, since we are not interested in volume variations leading to buckling:

$$(67)\ \Rightarrow\ a_n\{\omega_n{}^2+\frac{(n+1)(n-1)(n+2)}{W_e}+(n+1)\left[\left(-\frac{1}{3}\right)(-12)+\frac{4\omega_n}{Re_s}+B\left(n^2(n+1)^2-(1-v)n(n+1)\right)\right]\}+$$

$$+b_n(n+1)\left\{(-2)n(n+1)-\frac{2\omega_n}{Re_s}(n+1)n-B[\lambda_n^2-(1-v)\lambda_n]\right\}=0 \quad (69)$$

$$(68)\Rightarrow \left[-2-\frac{2\omega_n}{Re_s}+B[(1-v)-n(n+1)]\right]a_n+b_n\left[-\frac{2-4n(n+1)}{3}-\frac{2(1-n(n+1))\omega_n}{Re_s}-\right.$$

$$\left.B[(1-v)-n(n+1)]\right]=0 \quad (70)$$

Where four new terms are introduced: A_{11}, A_{12}, A_{21} and A_{22} as:

$$A_{11}=\omega_n{}^2+4(n+1)+\frac{(n+1)(n-1)(n+2)}{W_e}+\frac{4(n+1)\omega_n}{Re_s}+B(n+1)n[n(n+1)-(1-v)] \quad (71)$$

$$A_{12}=-2n(n+1)^2-\frac{2\omega_n}{Re_s}n(n+1)^2-Bn(n+1)^2[n(n+1)-(1-v)] \quad (72)$$

$$A_{21}=-2-\frac{2\omega_n}{Re_s}+B[(1-v)-n(n+1)] \quad (73)$$

$$A_{22}=-\frac{2-4n(n+1)}{3}-\frac{2(1-n(n+1))\omega_n}{Re_s}-B[(1-v)-n(n+1)] \quad (74)$$

In the next step, it is required that the determinant of the (67) and (68) system of equations to be zero and solve for ω_n thus allowing the eigenfrequencies of the particular problem to be evaluated. So we solve for: $A_{11}*A_{22}-A_{12}*A_{21}=0$

$$-\omega_n{}^2\left\{\frac{2-4n(n+1)}{3}+B[(1-v)-n(n+1)]\right\}-$$

$$-\left\{4(n+1)+\frac{(n+1)(n-1)(n+2)}{W_e}+B(n+1)^2n[(n+1)n-(1-v)]\right\}*$$

$$*\left(\frac{2-4n(n+1)}{3}+B[(1-v)-n(n+1)]\right)-$$

$$-\{2n(n+1)+Bn(n+1)^2[n(n+1)-(1-v)]\}\{2+B[(n+1)n-(1-v)]\}=0\Rightarrow$$

$$\Rightarrow \omega_n{}^2=-\left\{4(n+1)+\frac{(n+1)(n-1)(n+2)}{W_e}+B(n+1)^2n[(n+1)n-(1-v)]\right\}-$$

$$-\left[2n(n+1)+Bn(n+1)^2[n(n+1)-(1-v)]\right]\frac{2+B[(n+1)n-(1-v)]}{\frac{2-4n(n+1)}{3}+B[(1-v)-n(n+1)]} \quad (75)$$

2.2. Static Buckling

Static Buckling of a microbubble is the loss of its sphericity when the bubble is subjected to an external compressive load. This effect doesn't necessarily happen when the microbubble is insonated, but instead is more relevant when the forcing frequency of the acoustic excitation is much smaller than the eigenfrequency of volume pulsations of the microbubble, a situation most commonly known as slow compression. Static Buckling takes place when the external overpressure that is applied on the microbubble surpasses a critical value, for given viscoelastic properties and equilibrium radius for that microbubble. When the external overpressure becomes higher than that critical threshold then the spherosymmetric

configuration requires higher energy content than the buckled axisymmetric state, leading to the deformation of the shell to a shape governed by a Legendre eigenmode [2]. While the spherosymmetric configuration is solely composed of strain energy, the buckled state allows for both strain and bending energy to take place so the total elastic energy of the shell acquires a lower value. For small disturbances, the formula from which the external critical overpressure is provided is the following,:

$$P'_{cr} = \frac{2(3G_{3d})}{\sqrt{3(1-\nu^2)}}\left(\frac{\delta_s}{R_{eq}}\right)^2 \qquad (76)$$

Then, by letting

$$w_n = a_n e^{\omega_n t},\ \psi_n = \beta_n e^{\omega_n t}$$

And substituting in Equations (65) and (66), we obtain an eigenvalue problem of the form

$$\underline{\underline{A}}[\omega_n; R(P_{cr}), B, B, Re_s, \nu, n] * \begin{bmatrix}\alpha_n \\ \beta_n\end{bmatrix} = 0$$

And more specifically the set of equations presented below:

$$a_n\left\{{\omega_n}^2 + \frac{(n+1)(n-1)(n+2)}{W_e R^3} + \frac{n+1}{R}\left[\frac{\chi\left[2\left(R^2+1\right)-\left(R^2-1\right)(2-\lambda_n)\right]}{2(1-\nu)R^3} + \frac{4\omega_n}{Re_s R^2} + \frac{k_B}{R^4}\left[{\lambda_n}^2 - \lambda_n(1-\nu)\right]\right]\right\} +$$

$$+B_n\left\{\frac{-\chi\lambda_n\left(R^2+1\right)}{2(1-\nu)R^3} - \frac{2\lambda_n\omega_n}{Re_s R^2} - \frac{k_B}{R^4}\left[{\lambda_n}^2 - \lambda_n(1-\nu)\right]\right\}\frac{(n+1)}{R} = 0 \qquad (77)$$

$$a_n\left[\frac{-\chi\left(R^2+1\right)}{2R^3(1-\nu)} - \frac{2\omega_n}{Re_s R^2} + \frac{k_B}{R^4}(1-\nu-\lambda_n)\right] +$$

$$+B_n\left[\frac{-\chi}{2R^3(1-\nu)}\left[R^2\frac{2(1-\lambda_n)+1-\nu}{1+\nu} - 1\right] - \frac{2}{Re_s R^2}(1-\lambda_n)\omega_n - \frac{k_B}{R^4}(1-\nu-\lambda_n)\right] = 0 \qquad (78)$$

In order for the above set of equations to have a non trivial solution, its determinant must vanish,

$$\det\left\{\underline{\underline{A}}[\omega_n; R(P_{cr}), B, B, Re_s, \nu, n]\right\} = 0$$

which in turn provides the eigenvalues of the problem.

2.2.1. The Static Buckling Algorithm and its Initial Values

In order to be able to estimate the $P_{critical}$ for a certain contrast agent at varying radii, the viscoelastic properties of the contrast agent are required as well as, in the case where prestress was applied, the amount of prestress. After the viscoelastic properties were properly selected, a procedure of trial and error took place through which the stability of the contrast agent was evaluated. The range of radii that were examined was from 1.5 μm to 5μm and the eigenmodes listed were the Legendre modes P2 to P6. The main variable of the problem was

the ratio of the compressed bubble radius to the initial radius of the spherical bubble through which the critical pressure was later calculated. As soon the ratio dropped below a certain threshold, the solutions of the eigenvalue problem indicate that the microbubble becomes unstable. By repeating this process for the rest of the eigenmodes for a given initial radius, $P_{critical}$ values for each mode were obtained. After the stability analysis was completed, in order to find the sound amplitude for which the $P_{critical}$ was achieved the following equation was used:

$$P'_g V'^{\gamma} = P'_{g,0} V'^{\gamma} \qquad (79)$$

coupled with the condition for static equilibrium, i.e eq(3).

For slow compression, the pressure excitation is better simulated by a disturbance:

$$P'_{\infty} = P_{st}\left[1 + \varepsilon \cos\left(\omega'_f t'\right)\right] \qquad (80)$$

In the limit as ω_f tends to zero and after the initial transient has elapsed, the step change in the static pressure of the host fluid $P'_{\infty} = P_{st}(1 + \varepsilon)$ is simulated and the buckling behavior is recovered.

By substituting $P_{critical}$ as P'_{∞} in the equation $P'_{\infty} = P_{st}(1 + \varepsilon)$ and solving for ε, the sound amplitude for criticality was obtained. This procedure was repeated for the whole range of radii resulting in finding the sound amplitudes for the Pcriticals in each radius for every mode under consideration. Finally in order to obtain the curve for the static stability, the chosen mode for each radius was the one that required the lowest sound amplitude, meaning that mode would become present and excited before any other causing the loss of spherosymmetry in the microbubble. That allowed for the curve of Static Buckling to be plotted in the R0-ε Plane.

2.4. Parametric shape mode excitation and Dynamic Buckling

For growth of shape modes to be detected the procedure followed was quite different. An iterative parametric method took place where a computational algorithm was applied.

The main objective of the algorithm is to figure out the sound amplitude for which shape instabilities begin to occur for a certain contrast agent. In order for that to happen, an input of the viscoelastic and geometric properties of the microbubble as well as the environmental parameters was required. A range of radii and sound amplitudes was selected and for each pair of values in the radius amplitude plane, and given shell properties and forcing frequency, a time integration procedure took place in order to examine the evolution of the different shape modes. To this end eq (7) that describes the radial pulsations, R(t), of a microbubble was solved along with eq's (65) and (66) for the evolution of $w_n(t)$ and $\psi_n(t)$. For the case of parametric mode excitation to be examined the smallest amplitude for a certain mode to be excited was investigated, alternatively one can perform Floquet analysis [2], whereas for the onset of dynamic buckling a certain small number of periods of the forcing was set, e.g. 6 periods of the forcing frequency, and subsequently the critical sound amplitude was registered for which shape mode excitation occurred.

2.4.1 Initial Values and Algorithm

The method utilized had a few steps. Initially, the viscoelastic properties of the microbubble, the surrounding fluid and the sonic disturbance were given.

The thickness of the shell was considered to be 1nm. The bending elasticity of the membrane k_B is equal to $3*10^{-14}$ N m. The three dimensional shell shear modulus G_{3d} being $40*10^6$ N/m^2, $80*10^6$ N/m^2 and $160*10^6$ N/m^2 and all of those cases were examined separately. The three dimensional dilatational viscosity μ_{sk3d} of the membrane was set to 20 Pa s. The three dimensional shear viscosity μ_{sh3d} of the membrane was given two values during the computational experiments. It was set to 20 Pa s and 1 Pa s in order to observe what happens when the two viscosities are on the same level of value or not respectively. Poisson ratio v was set equal to 0.5 and the polytropic constant was set equal to 1.07.

The density of the surrounding liquid was taken to be that of water's i.e. 998 kg/m^3 while the viscosity was given the value of 0.001 Pa s. The sound velocity C_l is equal to 1540 m/s but, in order to compare with numerical simulations for which incompressibility was assumed, in the present study C_l was set to infinity. Three separated cases for the forcing frequency were selected: 1.0 MHz, 1.2 MHz and finally 1.7 MHz, while the static far field pressure was taken to be that of the atmosphere equal to 101325 Pa. In order to study the effect of prestress on the microbubbles the initial radius R was set to be lower than the stress free radius R_0 signifying an initial loss of the enclosed gas, possibly due to slow diffusion through the protective shell. The internal gas pressure was set so that the equilibrium of the normal stresses is satisfied along with the adiabatic gas law in the manner described in the previous subsection.

After configuring this initial input, there were three fields that needed to be defined to begin the simulations: a range of radii, a range for sound amplitude and a specific shape mode that was investigated in order to obtain the critical sound amplitude for its excitation. The radii of the microbubbles was selected to range between 1.5 μm and 5 μm with the step for the radius set to 0.05 μm. The sound amplitude was checked for values between 0.3 and 8.5 with a step of 0.05. Finally, the shape modes that were investigated were the 2nd, 3rd, 4th, 5th and 6th Legendre modes. Those were the modes observed to mostly get excited in these conditions and therefore they were investigated.

After deciding which shape mode we want to investigate, the n value that identifies the Legendre polynomial is selected and the algorithm starts. The algorithm completes two main functions while running. It provides the radial position and speed of the membrane particles. In addition it performs time integration on the evolution of the amplitude of the nth component of the radial displacement w_n and the derivative ψ_n of the displacement in the azimuthal direction, eq (7),(65),(66).

This way the algorithm makes a sweep over every sound amplitude value from the desirable range until it hits the one where instabilities arise in the sense that w_n and ψ_n start growing. That process is repeated for all radii in the range of input so, in the end, every radius in question has a sound amplitude value assigned to it. That helps constructing the phase diagrams with the radius and amplitude values in the axes showing when the nth mode will appear. The stability procedure is described in the formulation presented above and is also explained in greater detail by Tsiglifis [1].

By running the algorithm explained above for each shape mode that is to be examined, enough information is collected to create a phase diagram. In the next chapter, the phase diagrams of the contrast agents investigated are presented along with some useful observations made about their general behavior.

3. RESULTS & DISCUSSION

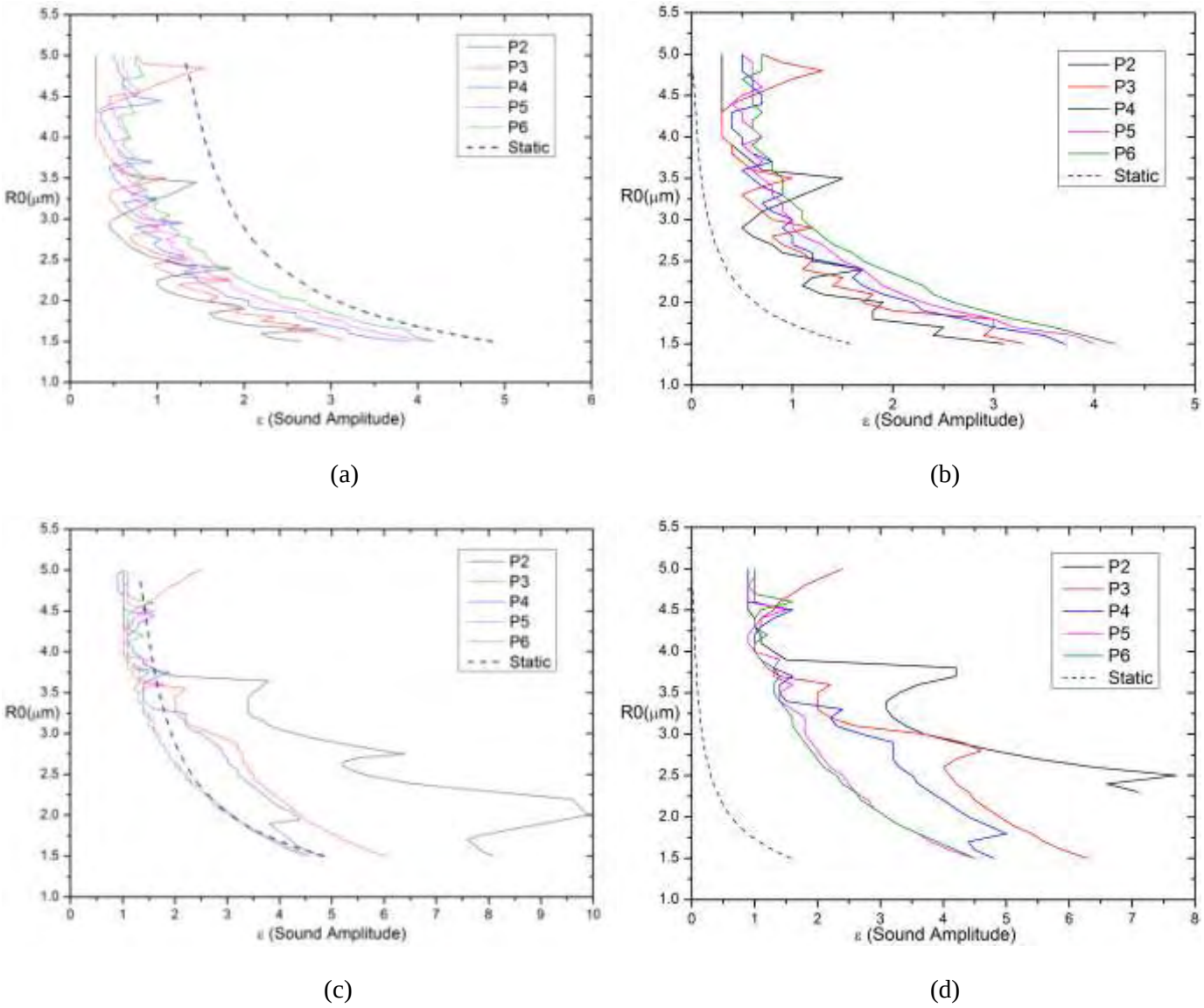

Figure 1. Phase Diagrams for the dynamic response subject to an external acoustic disturbance of a contrast agent insonated at 1MHz, with viscoelastic shell properties $G_s=40*10^6$ N/m^2, $\mu_s=20$ Pa*s and (a) $\mu_{shear}=1$ Pa*s without applying any prestress, (b) $\mu_{shear}=1$ Pa*s with the application of a 16.9% initial compression on the rest radius, (c) $\mu_{shear}=20$ Pa*s without applying any prestress and (d) $\mu_{shear}=20$ Pa*s with the application of a 16.9% initial compression on the rest radius.

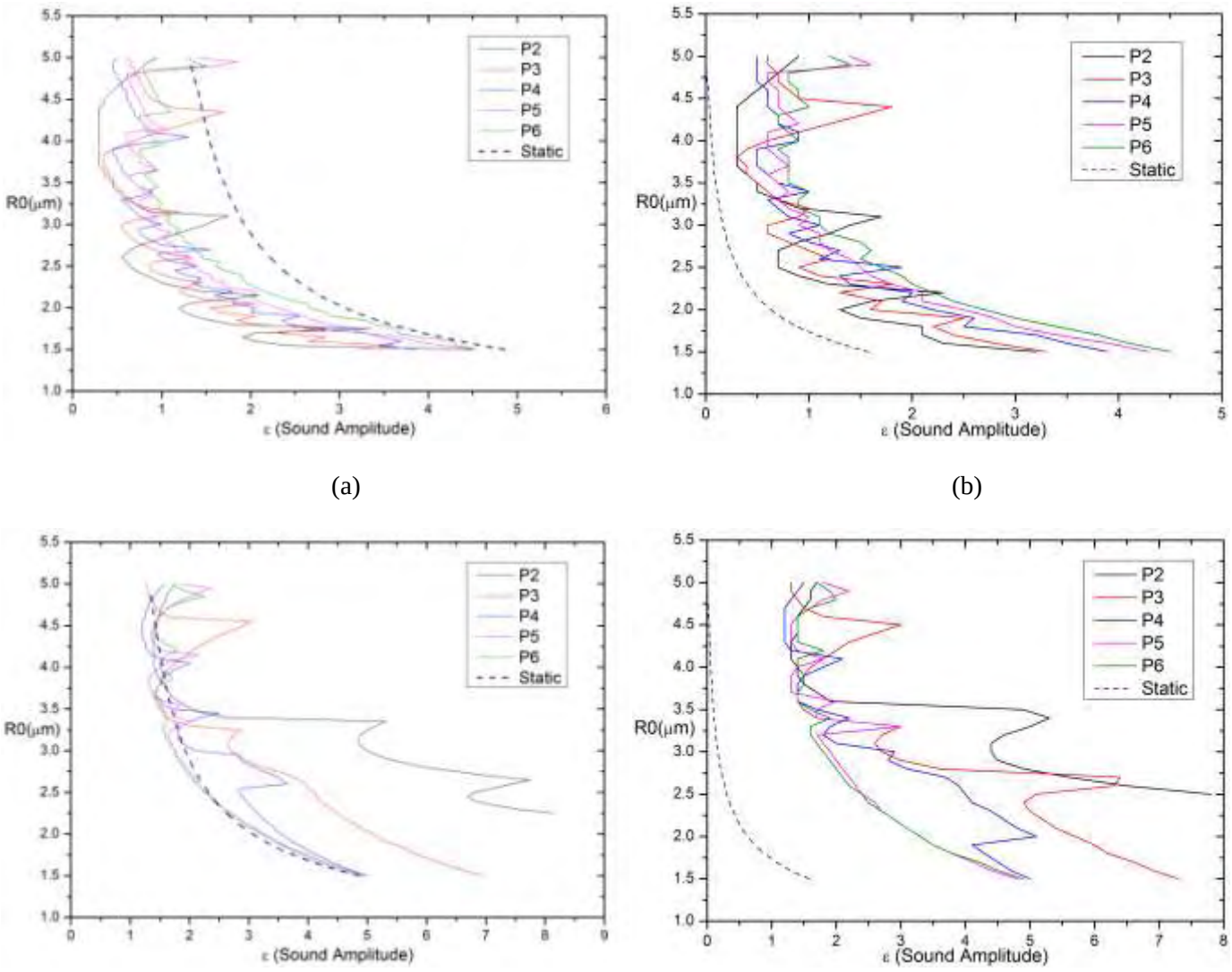

Figure 2. Phase Diagrams for the dynamic response subject to an external acoustic disturbance of a contrast agent insonated at 1.2MHz, with viscoelastic shell properties $G_s=40*10^6$ N/m^2, $\mu_s=20$ Pa*s and (a) $\mu_{shear}=1$ Pa*s without applying any prestress, (b) $\mu_{shear}=1$ Pa*s with the application of a 16.9% initial compression on the rest radius, (c) $\mu_{shear}=20$ Pa*s without applying any prestress and (d) $\mu_{shear}=20$ Pa*s with the application of a 16.9% initial compression on the rest radius.

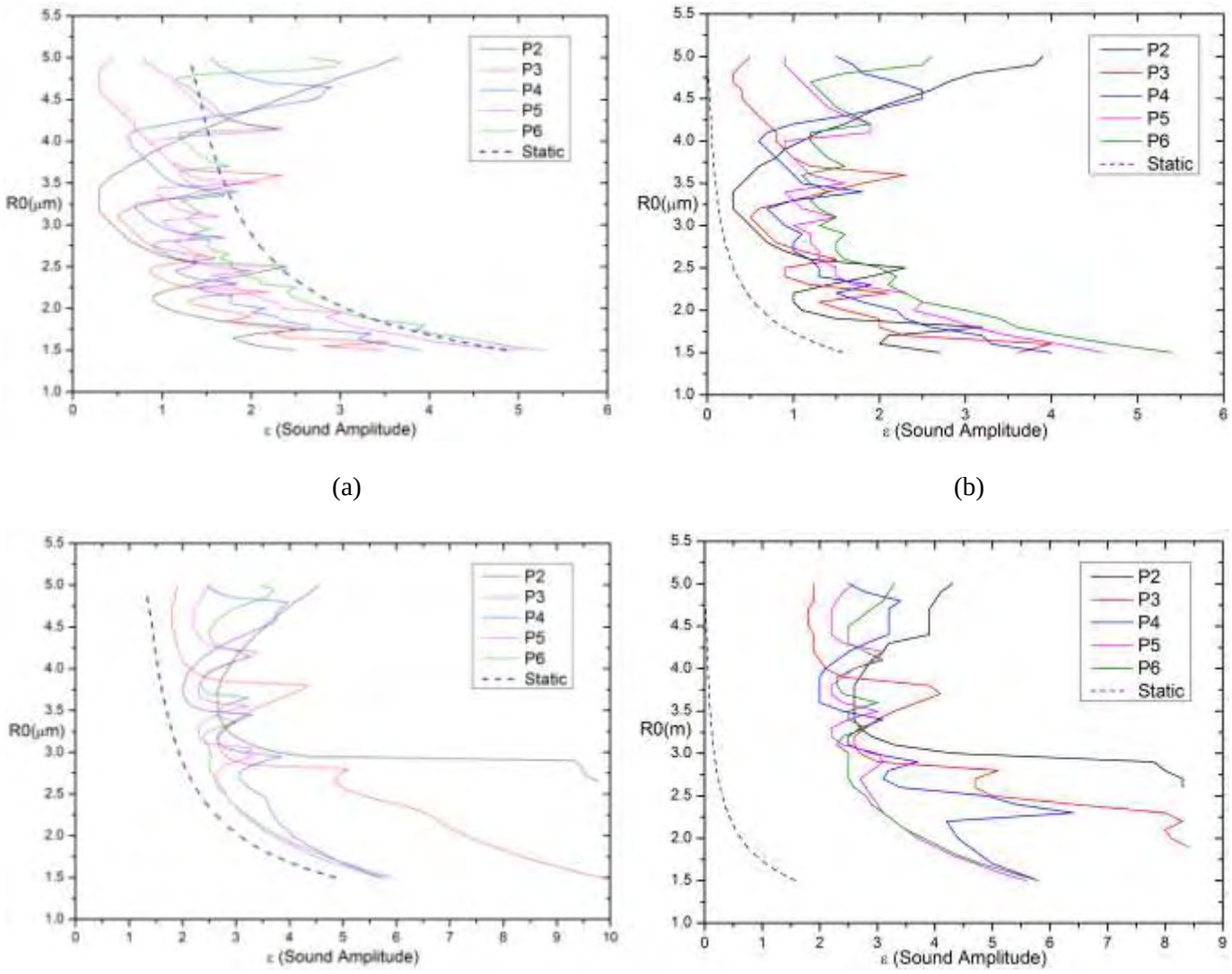

Figure 3. Phase Diagrams for the dynamic response subject to an external acoustic disturbance of a contrast agent insonated at 1.7MHz, with viscoelastic shell properties $G_s=40*10^6$ N/m^2, μ_s=20 Pa*s and (a) μ_{shear}=1 Pa*s without applying any prestress, (b) μ_{shear}=1 Pa*s with the application of a 16.9% initial compression on the rest radius, (c) μ_{shear}=20 Pa*s without applying any prestress and (d) μ_{shear}=20 Pa*s with the application of a 16.9% initial compression on the rest radius.

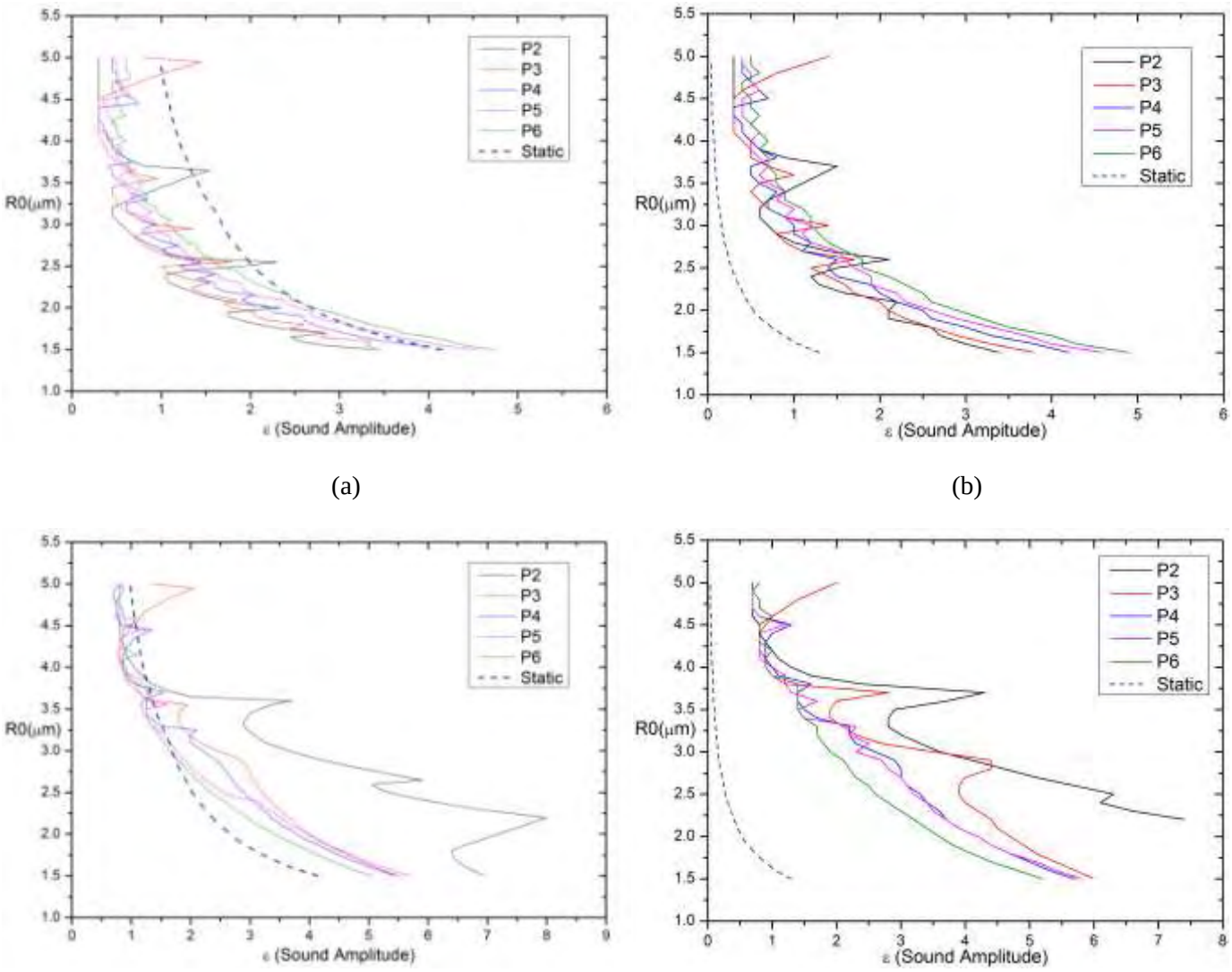

Figure 4. Phase Diagrams for the dynamic response subject to an external acoustic disturbance of a contrast agent insonated at 1MHz, with viscoelastic shell properties $G_s=80*10^6$ N/m^2, μ_s=20 Pa*s and (a) μ_{shear}=1 Pa*s without applying any prestress, (b) μ_{shear}=1 Pa*s with the application of a 12.8% initial compression on the rest radius, (c) μ_{shear}=20 Pa*s without applying any prestress and (d) μ_{shear}=20 Pa*s with the application of a 12.8% initial compression on the rest radius.

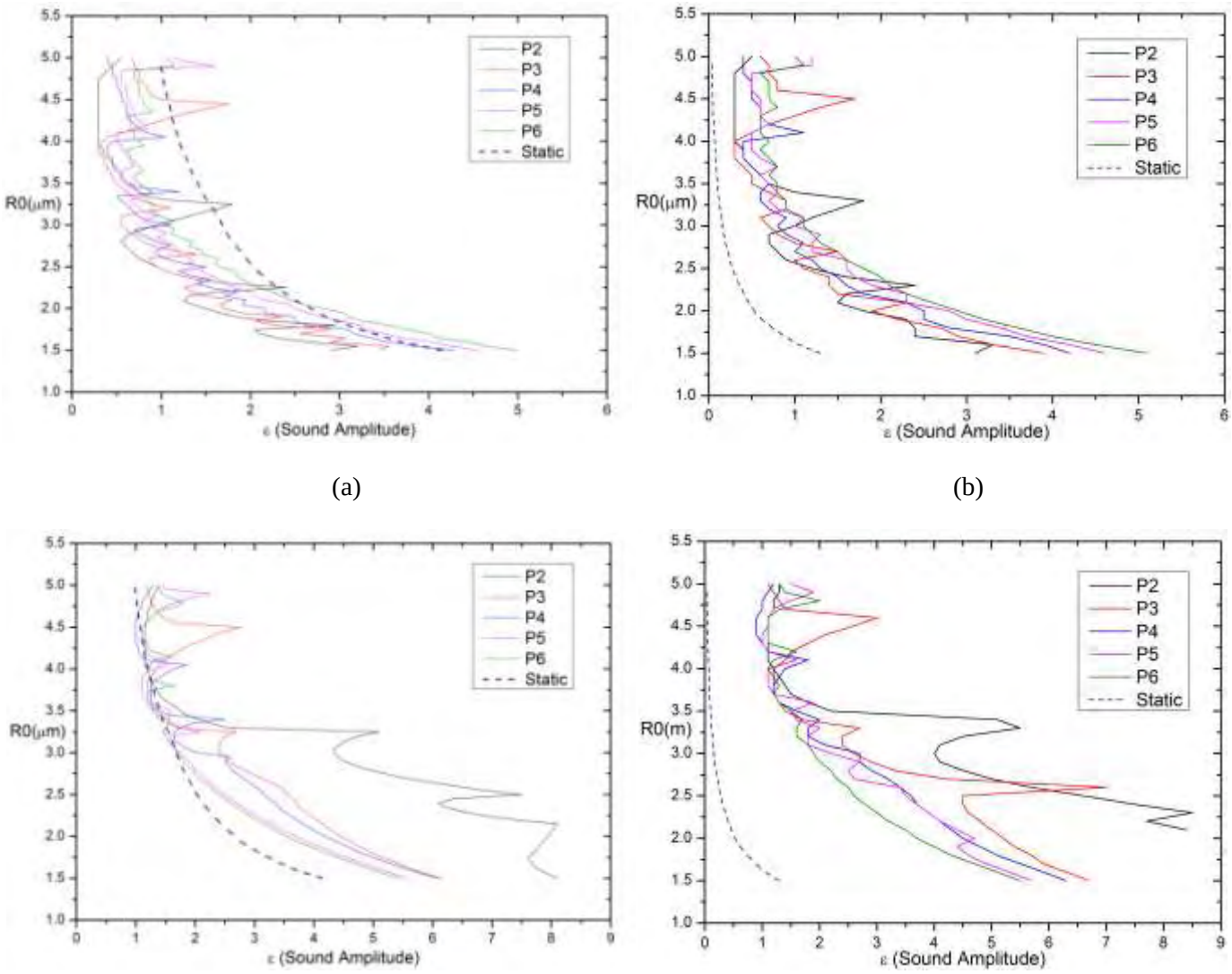

Figure 5. Phase Diagrams for the dynamic response subject to an external acoustic disturbance of a contrast agent insonated at 1.2MHz, with viscoelastic shell properties $G_s=80*10^6$ N/m^2, μ_s=20 Pa*s and (a) μ_{shear}=1 Pa*s without applying any prestress, (b) μ_{shear}=1 Pa*s with the application of a 12.8% initial compression on the rest radius, (c) μ_{shear}=20 Pa*s without applying any prestress and (d) μ_{shear}=20 Pa*s with the application of a 12.8% initial compression on the rest radius.

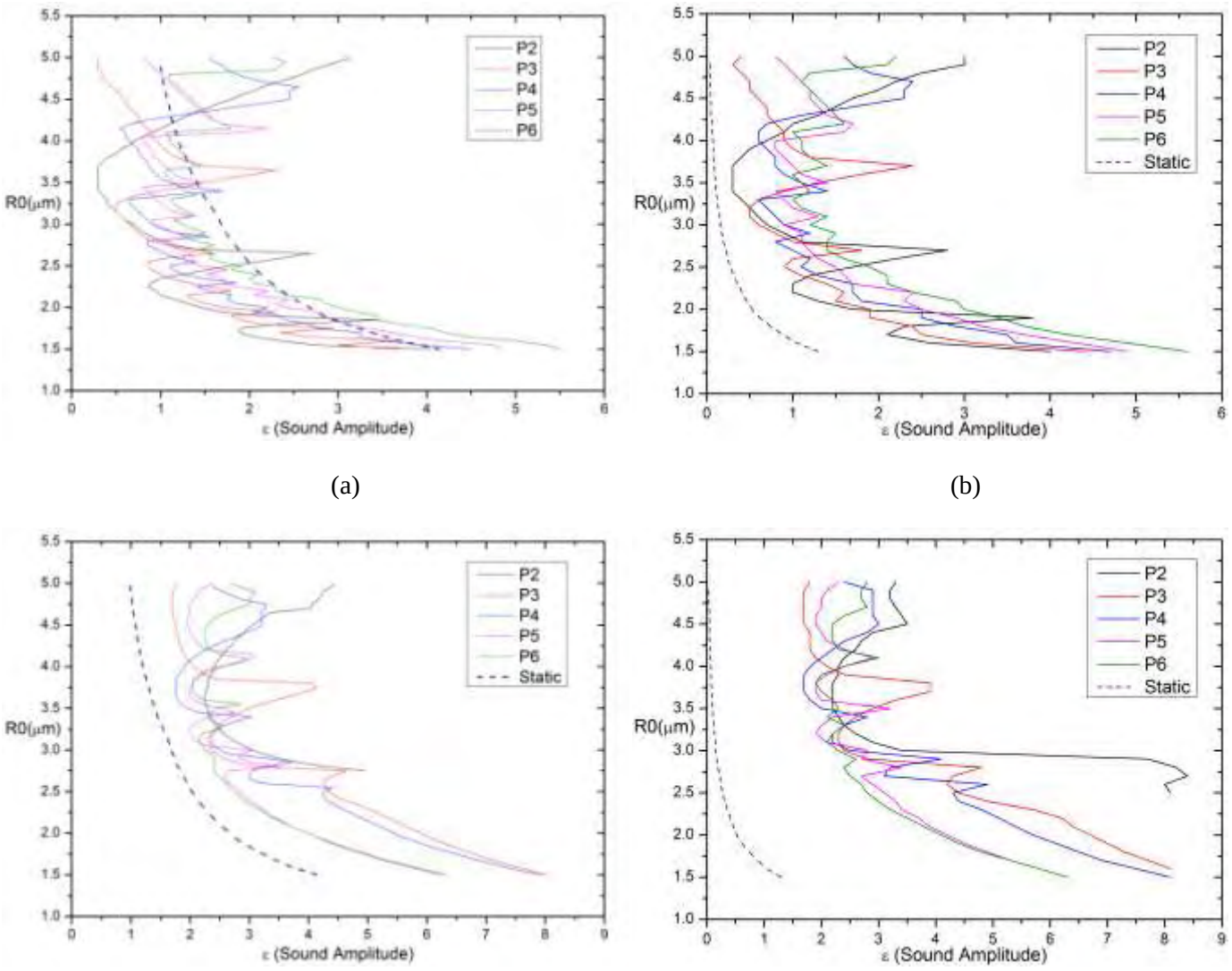

Figure 6. Phase Diagrams for the dynamic response subject to an external acoustic disturbance of a contrast agent insonated at 1.7MHz, with viscoelastic shell properties $G_s=80*10^6$ N/m^2, μ_s=20 Pa*s and (a) μ_{shear}=1 Pa*s without applying any prestress, (b) μ_{shear}=1 Pa*s with the application of a 12.8% initial compression on the rest radius, (c) μ_{shear}=20 Pa*s without applying any prestress and (d) μ_{shear}=20 Pa*s with the application of a 12.8% initial compression on the rest radius.

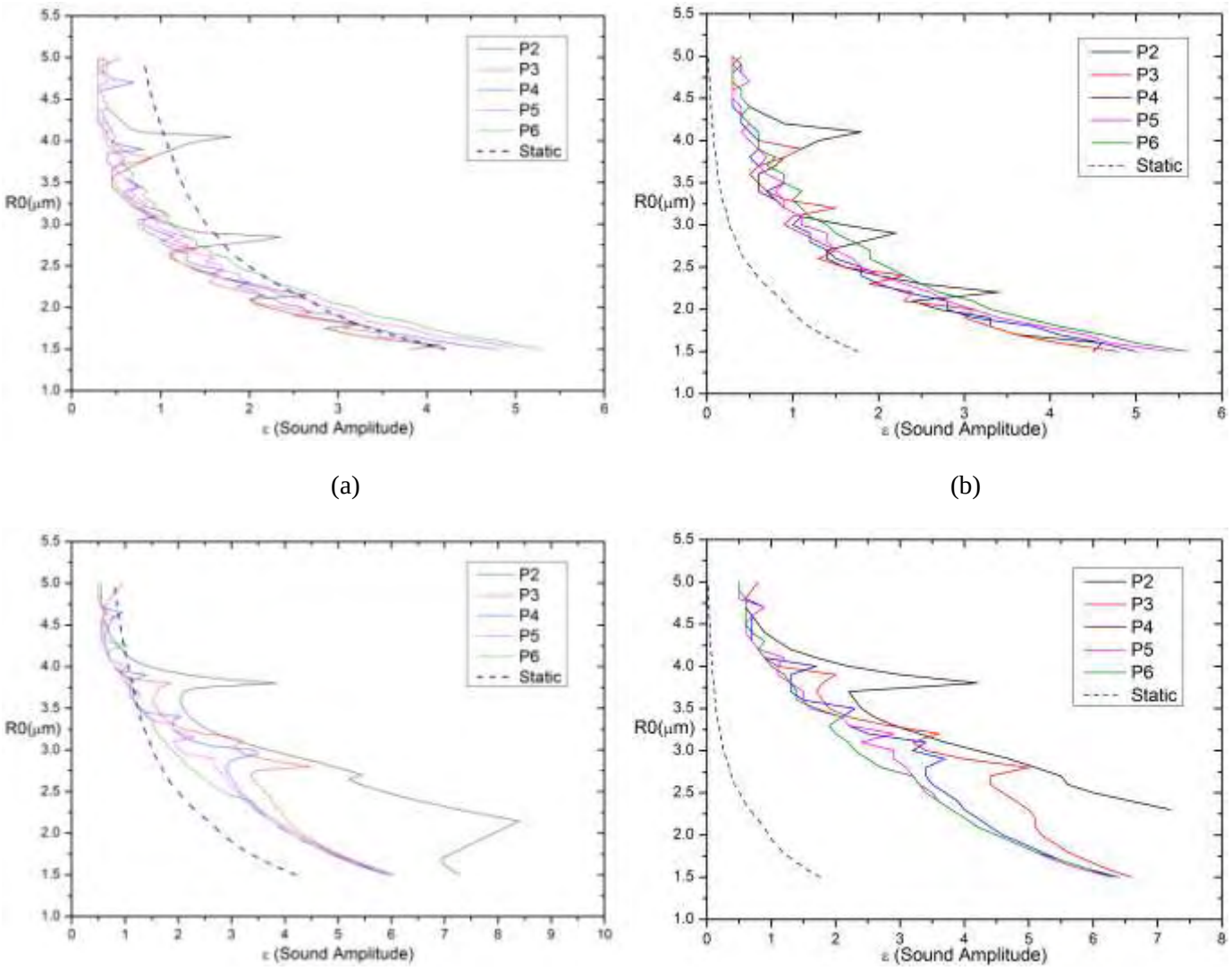

Figure 7. Phase Diagrams for the dynamic response subject to an external acoustic disturbance of a contrast agent insonated at 1MHz, with viscoelastic shell properties $G_s=160*10^6$ N/m^2, $\mu_s=20$ Pa*s and (a) $\mu_{shear}=1$ Pa*s without applying any prestress, (b) $\mu_{shear}=1$ Pa*s with the application of a 8.3% initial compression on the rest radius, (c) $\mu_{shear}=20$ Pa*s without applying any prestress and (d) $\mu_{shear}=20$ Pa*s with the application of a 8.3% initial compression on the rest radius.

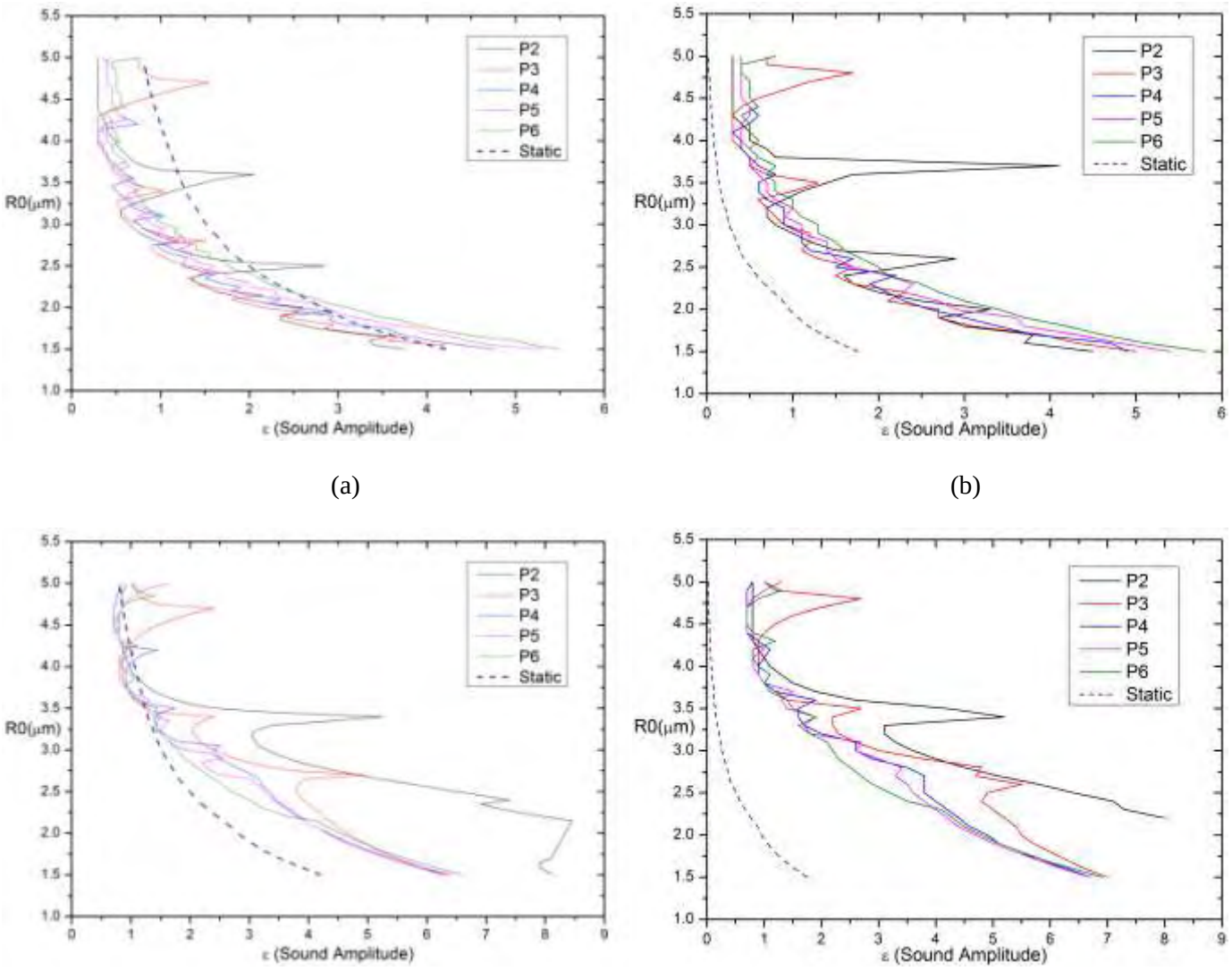

Figure 8. Phase Diagrams for the dynamic response subject to an external acoustic disturbance of a contrast agent insonated at 1.2MHz, with viscoelastic shell properties $Gs=160*10^6$ N/m^2, μ_s=20 Pa*s and (a) μ_{shear}=1 Pa*s without applying any prestress, (b) μ_{shear}=1 Pa*s with the application of a 8.3% initial compression on the rest radius, (c) μ_{shear}=20 Pa*s without applying any prestress and (d) μ_{shear}=20 Pa*s with the application of a 8.3% initial compression on the rest radius.

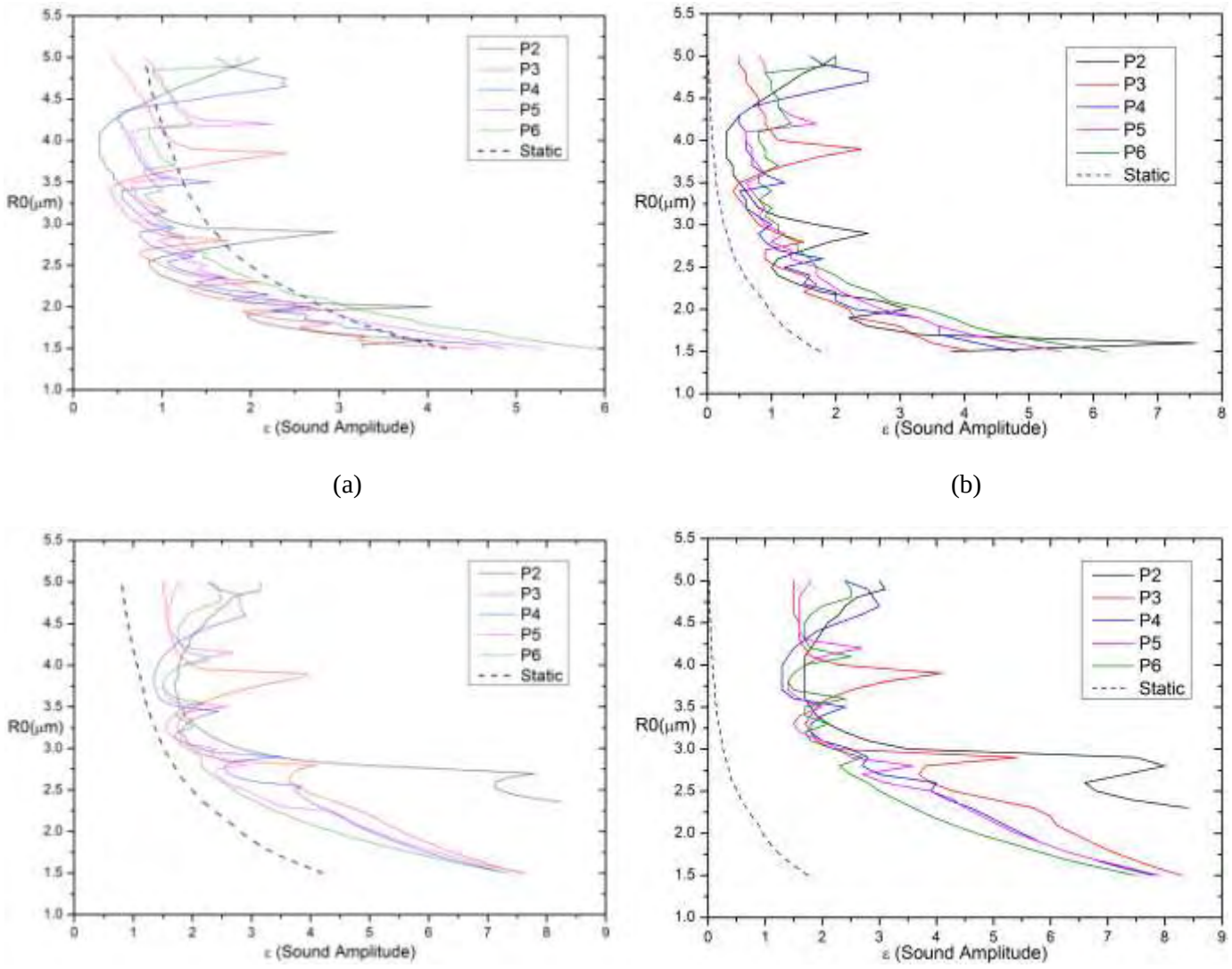

Figure 9. Phase Diagrams for the dynamic response subject to an external acoustic disturbance of a contrast agent insonated at 1.7MHz, with viscoelastic shell properties $G_s=160*10^6$ N/m^2, $\mu_s=20$ Pa*s and (a) $\mu_{shear}=1$ Pa*s without applying any prestress, (b) $\mu_{shear}=1$ Pa*s with the application of a 8.3% initial compression on the rest radius, (c) $\mu_{shear}=20$ Pa*s without applying any prestress and (d) $\mu_{shear}=20$ Pa*s with the application of a 8.3% initial compression on the rest radius.

In order to examine the effect that the prestress and the discrepancy between the shear and dilatational shell viscosity have on the critical thresholds for the onset for static buckling and for parametric mode excitation we first consider a stain softening shell with a shear modulus G_s=40MPa, a bending modulus $k_b = 3 \cdot 10^{-14} N \cdot m$, a thickness equal to 1nm and a dilatational shell viscosity of 20 Pa·s. The surface tension is set to 0.051 N/m, the polytropic ideal gas constant to γ=1.07 and the surrounding liquid is assumed to have the properties of water. In figures 1a,b it is presented the stability thresholds for a shear shell viscosity of 1Pa·s with no initial prestress and with an initial prestress of 16.9% compared to the stress free radius respectively, whereas in figures 1c,d the cases of equal shear and dilatational shell viscosities with no prestress and an initial prestressed state are shown respectively. In all figures the acoustic frequency is set to 1MHz. Upon examining the diagrams and comparing them with each other a few notable observations can be made regarding how each one of those parameters affects the behavior of the contrast agents. It is clear that the initial prestress of the bubble reduces significantly the thresholds for static buckling whereas it hardly affects the parametric mode excitation thresholds. The static curve of the prestressed contrast agents is moved to the left which means that static buckling happens for very low sound amplitudes when prestress is exerted on the membrane and it usually takes place at smaller amplitudes than the amplitudes needed for shape mode excitation. On the other hand, as it is expected the difference between the two shell viscosities has no effect on the static buckling thresholds and reduces only the thresholds for parametric mode excitation. When the two shell viscosities are equal, fig 1c, it can be seen that the sound amplitudes for parametric excitation are increased compared to the different shell viscosities of fig. 1a, especially for the smaller radii. It can also be noticed that the lesser the mode, the greater the increase in sound amplitude is and while in Fig 1a the mode curves of P2,P3,P4,P5 and P6 are in close proximity, in Fig 1c the modes are getting further apart, especially for the smaller radii.

In figures 2 and 3 the diagrams that correspond to the same cases presented in figure 1 but for an acoustic disturbance of 1.2MHz and 1.7MHz respectively are given. The same overall pattern is observed as above. By comparing the diagrams of figure 1 and figures 2 and 3, it appears that the increase of the forcing frequency increases slightly the sound thresholds for parametric instability and it is also evident that when the frequency is higher the dynamic curves of the modes seem to be growing apart. In figure 1 the curves are all banded together and the limits in amplitude of the shape modes with the same radius are really close, letting them to arise one after another while upping the amplitude. This behavior is even more evident while comparing figures 1 to 2 and then to 3 and observing the higher and lower parts of the curves. In figure 3 the upper and lower parts of the curves have grown very far apart. This is especially obvious between graphs 3a and 3c where the shear viscosity is much lower than the dilatational. Let it be reminded at this point that the static curve is the same for figures 1a,c, 2a,c and 3a,c as the acoustic imposed frequency has no effect on the static buckling thresholds.

In order to better assess the effect that the shear viscosity of the membrane has in the mode excitation four additional graphs are presented, figs 10a,b,c,d. A single radius equal to 3.6 μm has been selected and the forcing frequency of the simulation has been set to 1.2 MHz. The surface shear modulus for the samples has been set to 40 and 80 MPa. These graphs depict the change of the sound amplitude as the shear viscosity of the membrane gradually increases from a low value to that of the dilatational. From a first glance it becomes apparent that the shear viscosity has a direct impact on the sound amplitude for parametric mode excitation. For all the shape modes under observation, it is seen that the sound amplitude for excitation rises

along with the value of the shear viscosity. There is constant rise of the sound amplitude for all the modes, apart from the fifth one where in a few areas of the diagrams without prestress, a reduction of the amplitude takes place. Other than that, the second and the fifth modes seem to be the ones that experience the biggest raise. The surface shear modulus doesn't seem to affect the modes that much since the values of the sound amplitudes don't change that much with the exception of the fifth mode. Overall it is observed that the sound amplitude for parametric instability increases by raising the shear viscosity of the membrane.

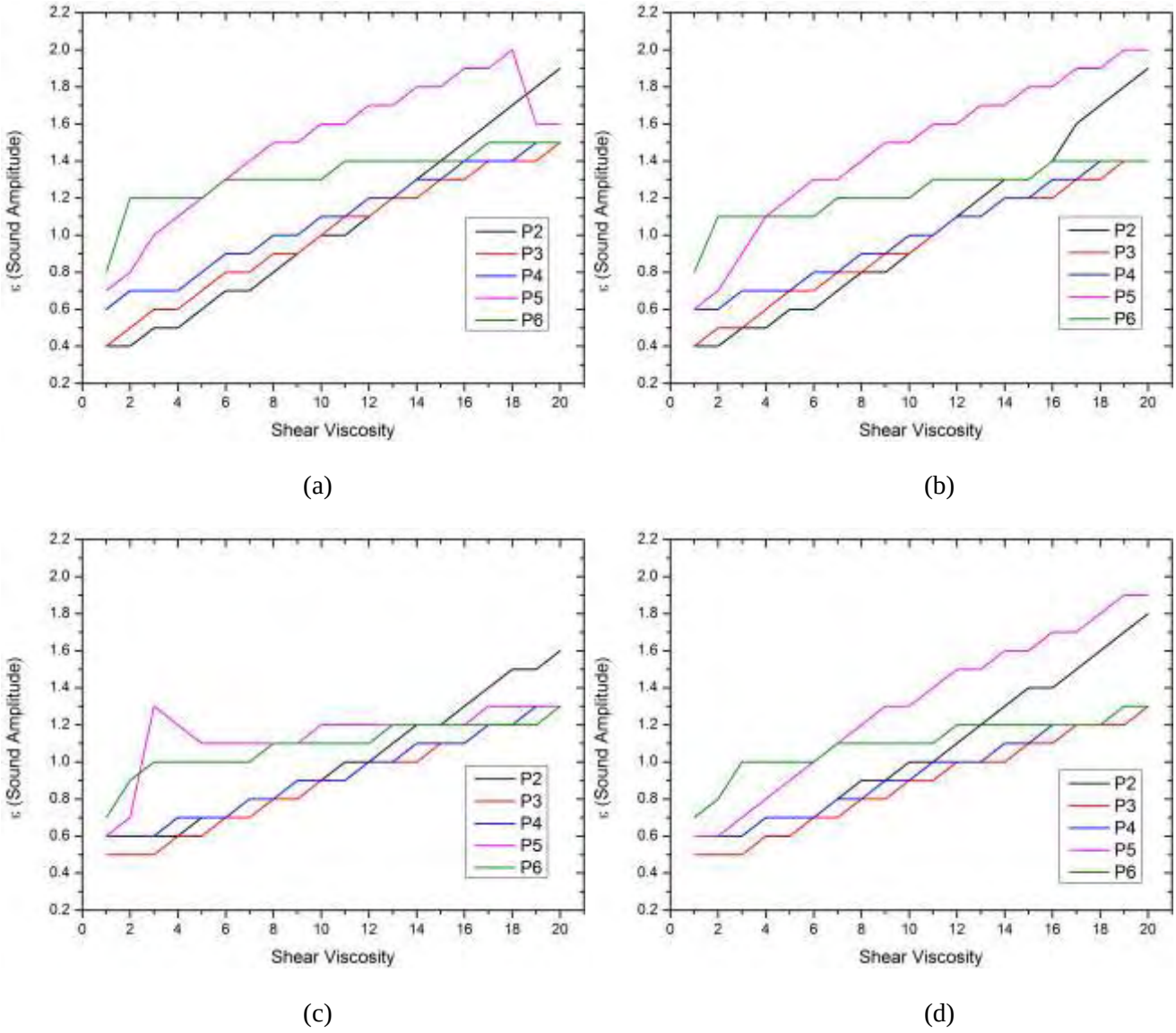

Figure 10. Phase Diagrams for the dynamic response subject to an external acoustic disturbance of a contrast agent insonated at 1.2MHz, with dilatational viscosity μ_s=20 Pa*s at radius=3.6μm and (a) $G_s=40*10^6$ N/m^2 without applying any prestress, (b) $G_s=40*10^6$ N/m^2 with the application of a 16.9% initial compression on the rest radius, (c) $G_s=80*10^6$ N/m^2 without applying any prestress and (d) $G_s=80*10^6$ N/m^2 with the application of a 12.8% initial compression on the rest radius.

We proceed to investigate the effect that the prestress and the discrepancy between the shear and dilatational shell viscosity have on the stability of harder shells. For this reason we consider the same contrast agent as above and we examine two different shear modules, Gs=80MPa and G_s=160MPa. In figures 4-6 it is presented the case of Gs=80MPa for frequencies 1, 1.2 and 1.7MHz respectively, whereas the same cases are shown in figures 7-9 for the case of Gs=160MPa. The amount of prestress applied on each microbubble depends on the surface shear modulus of its membrane. It should be noted that it was necessary to reduce the prestress exerted on microbubbles with higher G_s so that the membrane wouldn't buckle instantly due to the intensity of the loads since the critical threshold for static buckling reduces as the shell becomes harder. So for Gs equal 80 and 160 the prestress applied was 12.8% and 8.3% respectively.

Firstly, we focus on figures 4-6 that correspond to a shear modulus of 80MPa and we observe that the static curve is moved a bit to the left when compared with figures 1-3 meaning that static buckling occurs for even lower values of sound amplitude. An additional reduction is observed when the shear modulus is increased on 160MPa, figs 7-9.. It is also noted that for the case of shear modulus $80*10^6$ N/m^2, for equal shear and dilatational shell viscosities (meaning fig 4c, 5c and 6c) the static buckling occurs before the parametric mode excitation for small radii meaning about below 2.8μmFor the case of the further increased shear modulus $160*10^6$ N/m^2 and with no discrepancy between shell viscosities (meaning fig 7c, 8c and 9c) static buckling occurs before parametric mode excitation for small radii meaning about below 3.5μm. Nevertheless, in all cases when an initial prestressed state is considered the thresholds for static buckling are significantly decreased, whereas the difference between the two shell viscosities reduces only the thresholds for parametric mode excitation.

To sum up, by examining separately four different parameters i.e. the prestress, the forcing frequency, the shear viscosity and the surface shear modulus, we can observe common themes in the behavior of the contrast agents. More specifically:

Prestress	Prestress doesn't affect dynamic modes that much. The most drastic change that appears when comparing the diagrams with prestress and those without, is the static curve. In microbubbles where prestress is applied, static buckling occurs for much lower sound amplitudes.
Shear Viscosity, μ_s	By increasing the shear viscosity from a low value to equal that of the dilatational viscosity, it appears to increase the sound amplitude needed for mode excitation. Some modes seem to be affected more than others.
Forcing Frequency, v_f	By increasing the forcing frequency, an increase of the required sound amplitude for mode excitation follows, plus the curves of each mode seem to be growing further apart. That means that the excitation of multiple shape modes becomes harder to achieve.
Surface Shear Modulus, G_s	By increasing the surface shear modulus G_s, the amplitude values of the static curve seem to drop (movement to the left). Greater decrease is witnessed while changing from 40 to 80 than when changing from 80 to 160. This change is more apparent to the diagrams without the application of prestress. It also increases the required amplitude of the parametric mode excitation curves to appear even further.

4. CONCLUSIONS

The main objective of this thesis was the construction and evaluation of phase diagrams of coated microbubbles when those are subjected to specific conditions. Those microbubbles have a gas core, which is assumed to be comprised of ideal gas, and are coated by a thin viscoelastic membrane made of lipids. The encapsulated bubble is surrounded by an ideal incompressible liquid.

The phase diagrams of such microbubbles are illustrated in an R_0-ε space and depict the circumstances of appearance of shape modes. Shape modes are geometrical configurations that the microbubble assumes in order to minimize the total elastic energy of the shell. Once a particular contrast agent becomes insonated, it starts to oscillate spherosymmetrically. If the sound amplitude of the pressure wave exceeds a certain threshold, shape mode excitation takes place and the microbubble enters a buckled state. The phase diagrams show the relationship between the radius of a microbubble and the sound amplitude required for a specific shape mode to be excited.

To achieve the construction of such diagrams, rheological models were used that described the stresses and forces that strained the shell of the microbubble as well as the deformation that the shell went under. The models used were those for Mooney-Rivlin and Neo-Hookean membranes, meaning the ones that had a strain softening shell, focusing mostly on Neo-Hookean membranes. Using the formulation presented in the above segment, two pieces of code were created, one in a Mathematica computational environment and one in ForTran, describing the static buckling and the parametric mode excitation respectively.

The codes mentioned worked as intended and produced the required results for the diagrams to be successfully constructed. The parametric analysis that took place after that involved mainly four different variables. More specifically them being: the prestress exerted on the shell, the shear viscosity of the shell, the forcing frequency of the sound waves and the surface shear modulus of the membrane. By comparing and contrasting the results with each other, some rather interesting conclusions were drawn regarding the behavior of contrasts agents that had both different viscoelastic properties and acoustic stimuli.

In all cases examined during the presentation of the results, the contrast agents were behaving quite similarly when the same circumstances where imposed leading to the belief that the variables mentioned above affect the shape mode excitation in specific ways. A brief repetition of the conclusions drawn follows.

The prestress exerted on the microbubble has a major role in the appearance of the static shape modes since it seems that while the prestress increases, the sound amplitude required is reduced for static buckling signicantly. However it doesn’t seem to affect the parametric excitation of the shape modes.

The membrane’s shear viscosity is linked directly to the sound amplitude that is required for mode excitation since while the shear viscosity of the shell increases, the sound amplitude is increased as well.

Regarding the forcing frequency and the surface shear modulus, as they increase, the sound amplitude of the sound waves slightly increases. The static buckling threshold is observed to decrease slightly while the surface shear modulus is increased. In addition, the forcing

frequency increase, causes the different shape modes curves to grow further apart, and with the shear modulus increasing, the static buckling seems to be taking place for lower sound amplitudes.

The construction of the aforementioned phase diagrams provided some insight as to how differently manufactured contrast agents react when they get insonated and it allowed a prediction as to when certain shape modes may arise. By utilizing the codes mentioned, an even further exploration of the encapsulated microbubbles' behavior might be eligible thus allowing greater understanding of their nature and enabling the creation of more suitable agents for specific biomedical and further applications.

BIBLIOGRAPHY

[1] K.A. Tsiglifis, *Numerical Simulation of Bubble Dynamics in Response to Acoustic Disturbances,* (2007).

[2] K.Tsiglifis and N.A. Pelekasis, "Parametric stability and dynamic buckling of an encapsulated microbubble subject to acoustic disturbances," (2011).

[3] J. S. Allen, D. J. May, and K. W. Ferrara, "Dynamics of therapeutic ultrasound contrast agents," Ultrasound Med. Biol. **vol. 28**, 805 (2002).

[4] B. Dollet, S. M. van der Meer, V. Garbin, N. De Jong, D. Lohse, and M. Versluis, "Nonspherical oscillations of ultrasound contrast agent microbubbles," Ultrasound Med. Biol. **vol. 34**, 1465 (2008).

[5] S. Zhao, K. W. Ferrara, and P. Dayton, "Asymmetric oscillation of adherent targeted ultrasound contrast agents," Appl. Phys. Lett. **vol. 87**, 134103 (2005).

[6] P. Marmottant and S. Hilgenfeldt, "Controlled vesicle deformation and lysis by single oscillating bubbles," Nature London **vol. 423**, 153 (2003).

[7] M. Postema, A. van Wamel, F. J. ten Cate, and N. de Jong, "High-speed photography during ultrasound illustrates potential therapeutic applications of microbubbles," Med. Phys. **vol. 32**, 3707 (2005).

[8] A. Bouakaz, M. Versluis, and N. de Jong, "High-speed optical observations of contrast agent destruction," Ultrasound Med. Biol. **vol. 158**, 129 (2005).

[9] K. Efthymiou, N. Pelekasis, M. B. Butler, D. H. Thomas and V. Sboros, "The effect of resonance on transient microbubble acoustic response: Experimental observations and numerical simulations," (2018).

[10] S. R. Sirsi and M. A. Borden, "Microbubble compositions, properties and biomedical applications," *Bubble Science, Engineering & Technology,* **vol. 1**, no. 1-2, 3, (2009).

[11] E. Dressaire, R. Bee, D. C. Bell, A. Lips and H. A. Stone, "Interfacial polygonal nanopatterning of stable microbubbles," *Science*, **vol. 320**, no. 5880, 1198, (2008).

[12] R. E. Pattle, *Properties, function and origin of the alveolar lining layer [7],* **vol. 175**, 1125, (1955).

[13] S. Singhal, C. C. Moser and M. A. Wheatley, "Surfactant-Stabilized Microbubbles as Ultrasound Contrast Agents: Stability Study of Span 60 and Tween 80 Mixtures Using a Langmuir Trough," *Langmuir,* **vol. 9**, no. 9, 2426, (1993).

[14] S. H. Bloch, M. Wan, P. A. Dayton, and K. W. Ferrara, "Optical observation of lipid- and polymer shelled ultrasound microbubble contrast agents," Appl. Phys. Lett. **vol. 84**, 631 (2004).

[15] R. Notter and Z. Wang, "Pulmonary surfactant: Physical chemistry, physiology and replacement," *Reviews in Chemical Engineering, 13(4),* (1997).

[16] D. H. Kim, M. J. Costello, P. B. Duncan and D. Needham, "Mechanical properties and microstructure of polycrystalline phospholipid monolayer shells: Novel solid microparticles," *Langmuir,* **vol. 19**, no. 20, 8455, (2003).

APPENDIX A

In this part, the identities needed for the expansions of certain terms of the equations in formulation are presented.

$$H(\,) = \frac{\partial^2}{\partial\theta^2}(\,) + \cot(\theta)\frac{\partial}{\partial\theta}(\,) \tag{A1}$$

$$HH(\,) = \frac{\partial^2}{\partial\theta^2}\left(\frac{\partial^2}{\partial\theta^2}(\,) + \cot(\theta)\frac{\partial}{\partial\theta}(\,)\right) + \cot(\theta)\frac{\partial}{\partial\theta}\left(\frac{\partial^2}{\partial\theta^2}(\,) + \cot(\theta)\frac{\partial}{\partial\theta}(\,)\right) \tag{A2}$$

Operators H( ) and HH( ) are typically employed in classical axisymmetric shell theory in order to simplify the algebra by utilizing the useful properties of the Legendre polynomials P_n. [1],[2]

$$H(P_n) = -\lambda_n P_n \tag{A3}$$

$$HH(P_n) = {\lambda_n}^2 P_n \tag{A4}$$

$$\lambda_n = n(n+1) \tag{A5}$$

$$\frac{\partial^3}{\partial\theta^3}(\,) - (1 + cot^2\theta)\frac{\partial}{\partial\theta}(\,) + \cot(\theta)\frac{\partial^2}{\partial\theta^2}(\,) = -\lambda_n\frac{\partial}{\partial\theta}(\,) \tag{A6}$$